2014-09

Reactive power compensation using an energy management system

Prato, Michael V.

Monterey, California: Naval Postgraduate School

NAVAL POSTGRADUATE SCHOOL

MONTEREY, CALIFORNIA

THESIS

REACTIVE POWER COMPENSATION USING AN ENERGY MANAGEMENT SYSTEM

by

Michael V. Prato

September 2014

Thesis Advisor: Alexander L. Julian
Co-Advisor: Giovanna Oriti

Approved for public release; distribution is unlimited

THIS PAGE INTENTIONALLY LEFT BLANK

REPORT DOCUMENTATION PAGE

Form Approved OMB No. 0704–0188

1. AGENCY USE ONLY *(Leave blank)*	**2. REPORT DATE** September 2014	**3. REPORT TYPE AND DATES COVERED** Master's Thesis

4. TITLE AND SUBTITLE
REACTIVE POWER COMPENSATION USING AN ENERGY MANAGEMENT SYSTEM

5. FUNDING NUMBERS

6. AUTHOR(S) Michael V. Prato

7. PERFORMING ORGANIZATION NAME(S) AND ADDRESS(ES)
Naval Postgraduate School
Monterey, CA 93943–5000

8. PERFORMING ORGANIZATION REPORT NUMBER

9. SPONSORING /MONITORING AGENCY NAME(S) AND ADDRESS(ES)
N/A

10. SPONSORING/MONITORING AGENCY REPORT NUMBER

11. SUPPLEMENTARY NOTES The views expressed in this thesis are those of the author and do not reflect the official policy or position of the Department of Defense or the U.S. Government. IRB Protocol number ____N/A____.

12a. DISTRIBUTION / AVAILABILITY STATEMENT
Approved for public release; distribution is unlimited

12b. DISTRIBUTION CODE

13. ABSTRACT (maximum 200 words)

A significant contributor to higher energy costs and reduced energy efficiency is the reactive power demand on the grid. Inductive power demand reduces power factor, increases energy losses during transmission, limits real power supplied to the consumer, and results in higher costs to the consumer. Compensating for a reactive power demand on the grid by providing reactive power support to the power distribution system creates energy efficiency gains and improves cost savings.

One method of compensating for reactive power is by incorporating an energy management system (EMS) into the power distribution system. An EMS can monitor reactive power requirements on the grid and provide reactive power support at the point of common coupling (PCC) in the power distribution system in order to increase energy efficiency.

The use of an EMS as a current source to achieve a unity power factor at the grid is demonstrated in this thesis. The power factor angle was determined using a zero-crossing detection algorithm. The appropriate amount of compensating reactive current was then injected into the system at the PCC and controlled using closed-loop current control. The process was simulated using Simulink and then validated in the laboratory using the actual EMS hardware.

14. SUBJECT TERMS Reactive power, reactive power compensation, reactive power control, reactive power demand, power factor, power factor improvement, power factor correction, energy management system, EMS, power loss, reactive power loss, zero-crossing detection, closed-loop current control, energy efficiency, energy cost savings	**15. NUMBER OF PAGES** 77
	16. PRICE CODE

17. SECURITY CLASSIFICATION OF REPORT	**18. SECURITY CLASSIFICATION OF THIS PAGE**	**19. SECURITY CLASSIFICATION OF ABSTRACT**	**20. LIMITATION OF ABSTRACT**
Unclassified	Unclassified	Unclassified	UU

NSN 7540–01–280–5500

Standard Form 298 (Rev. 2–89)
Prescribed by ANSI Std. 239–18

THIS PAGE INTENTIONALLY LEFT BLANK

Approved for public release; distribution is unlimited

REACTIVE POWER COMPENSATION USING AN ENERGY MANAGEMENT SYSTEM

Michael V. Prato
Major, United States Marine Corps
B.S., University of Illinois, 2001

Submitted in partial fulfillment of the
requirements for the degree of

MASTER OF SCIENCE IN ELECTRICAL ENGINEERING

from the

NAVAL POSTGRADUATE SCHOOL
September 2014

Author: Michael V. Prato

Approved by: Alexander L. Julian
Thesis Advisor

Giovanna Oriti
Co-Advisor

R. Clark Robertson
Chair, Department of Electrical and Computer Engineering

THIS PAGE INTENTIONALLY LEFT BLANK

ABSTRACT

A significant contributor to higher energy costs and reduced energy efficiency is the reactive power demand on the grid. Inductive power demand reduces power factor, increases energy losses during transmission, limits real power supplied to the consumer, and results in higher costs to the consumer. Compensating for a reactive power demand on the grid by providing reactive power support to the power distribution system creates energy efficiency gains and improves cost savings.

One method of compensating for reactive power is by incorporating an energy management system (EMS) into the power distribution system. An EMS can monitor reactive power requirements on the grid and provide reactive power support at the point of common coupling (PCC) in the power distribution system in order to increase energy efficiency.

The use of an EMS as a current source to achieve a unity power factor at the grid is demonstrated in this thesis. The power factor angle was determined using a zero-crossing detection algorithm. The appropriate amount of compensating reactive current was then injected into the system at the PCC and controlled using closed-loop current control. The process was simulated using Simulink and then validated in the laboratory using the actual EMS hardware.

THIS PAGE INTENTIONALLY LEFT BLANK

TABLE OF CONTENTS

THIS PAGE INTENTIONALLY LEFT BLANK

LIST OF FIGURES

THIS PAGE INTENTIONALLY LEFT BLANK

LIST OF TABLES

THIS PAGE INTENTIONALLY LEFT BLANK

LIST OF ACRONYMS AND ABBREVIATIONS

AC	alternating current
DC	direct current
DG	distributed generation
DOD	Department of Defense
DON	Department of the Navy
FPGA	field programmable gate array
EMS	energy management system
IGBT	insulated gate bipolar transistor
IPM	integrated power module
JTAG	joint test action group
KCL	Kirchhoff's Current Law
LCD	liquid-crystal display
LPF	low-pass filter
NPS	Naval Postgraduate School
PC	personal computer
PCB	printed circuit board
PCC	point of common coupling
PF	power factor
PG&E	Pacific Gas and Electric
PI	proportional-integral
PLL	phase-locked loop
PWM	pulse width modulation
RMS	root mean square
USMC	United State Marine Corps
VAR	volt-ampere reactive
VARh	volt-ampere reactive hour
VSI	voltage source inverter

THIS PAGE INTENTIONALLY LEFT BLANK

EXECUTIVE SUMMARY

A significant contributor to higher energy costs and reduced energy efficiency in delivering power to the consumer is the reactive power demand on the grid. Inductive power demand reduces the power factor, increases energy losses during transmission, limits real power supplied to the consumer, and results in higher costs to the consumer due to increased power rating requirements on electrical equipment. Compensating for a reactive power demand on the grid by providing reactive power support to the power distribution system creates energy efficiency gains and improves cost savings.

One way to compensate for reactive power is to incorporate an energy management system (EMS) into the power distribution system. An EMS can monitor reactive power requirements on the grid and provide reactive power support at the point of common coupling (PCC) in the power distribution system in order to increase energy efficiency.

The use of an EMS as a current source to achieve a unity power factor at the grid is demonstrated in this thesis. The power factor angle was determined using a zero-crossing detection algorithm. The appropriate amount of compensating reactive current was then injected into the system at the PCC and controlled using closed-loop current control. The process was simulated using Simulink software and then validated using the actual EMS.

A schematic of the experimental EMS's power electronics is provided in Figure 1. Note that the EMS employs a single-phase H-bridge inverter consisting of two single-leg inverters. A third leg connects a DC power supply to the inverter via a bidirectional buck-boost converter. Pulse width modulation (PWM) with unipolar voltage switching delivers the H-bridge gate signals that create an EMS output current i_{ems}. A low-pass filter facilitates a clean signal at the output of the inverter. Note that reactive current i_{ems} flows through the filter inductor. For the purpose of this thesis, the H-bridge inverter is controlled as a current source using a programmable microcontroller that regulates the

polarity of the inverter output voltage and controls the flow of power using feedback provided by a sensor positioned at the load.

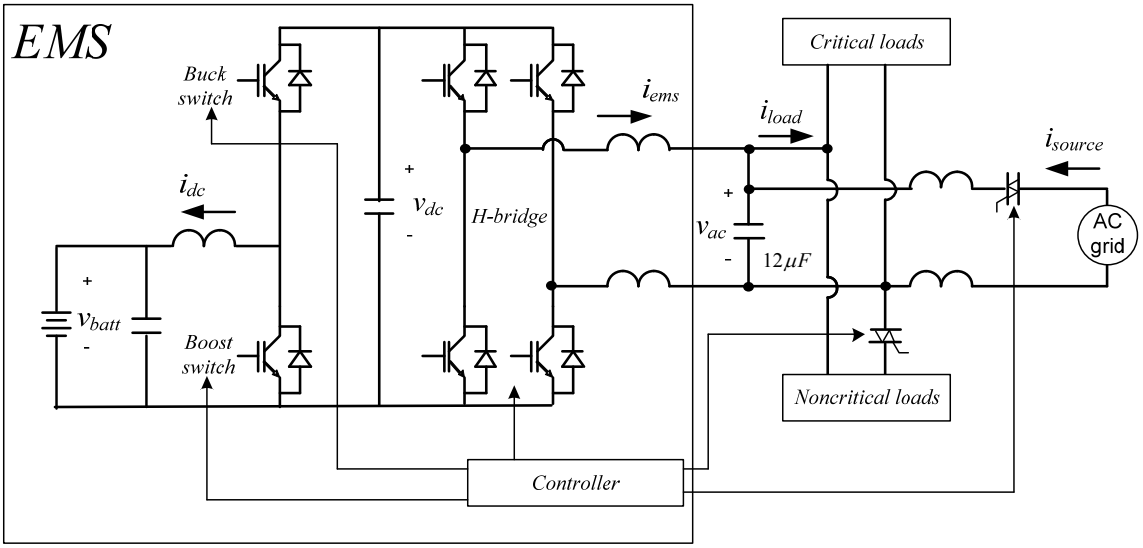

Figure 1. EMS power electronics schematic.

The EMS output current i_{ems} is controlled by a reactive power compensation program developed in Simulink that regulates the amount of reactive current injected into the system. The program employs a zero-crossing detection algorithm to determine the power factor angle φ_{source} at the grid. A power factor angle error correction algorithm eliminates any numerical error in the φ_{source} calculation that may result from transients in the source current i_{source}. Compensating i_{ems} is generated by the EMS and controlled using a PI controller that adjusts the amplitude of i_{ems} to drive φ_{source} to zero. This eliminates the reactive power demand on the grid by achieving a unity power factor.

The circuit used by Simulink to simulate this process is a streamlined version of the circuit shown in Figure 1. The simulation disregards the EMS's power electronics by modeling the EMS merely as a current source. A schematic of the equivalent circuit is provided in Figure 2. Modeling the EMS in this fashion assumes a clean sinusoidal i_{ems} signal from the H-bridge inverter without considering the PWM and closed-loop voltage control used to generate i_{ems}. This isolates i_{ems} in order to facilitate a focused examination of the Simulink-based power factor improvement methodology developed for the EMS.

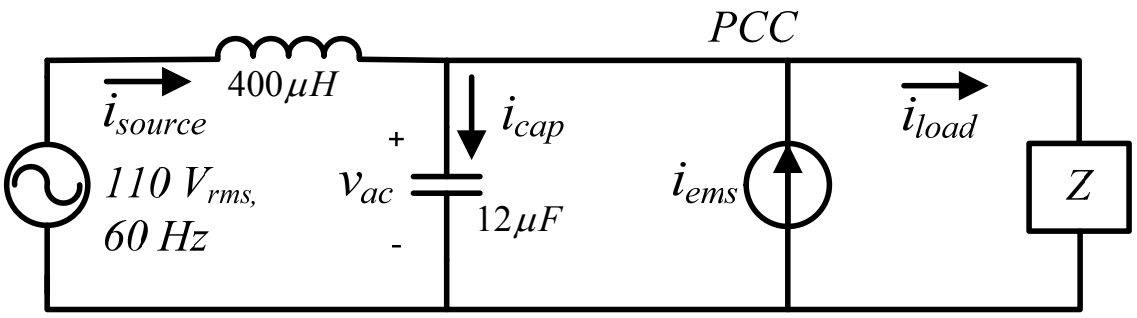

Figure 2. Streamlined circuit schematic.

A scenario is presented in Figure 3 in which an ohmic-inductive load is placed on the circuit at 0.25 sec into the simulation. This creates an overall inductive reactance in the circuit that demands reactive power from the grid, causing a lagging grid power factor of 75%. The EMS compensates by acting as a capacitive load in delivering magnetizing volt-amperes reactive (VAR) to the system via a capacitive i_{ems} that leads v_{source} by 90^0. The capacitive i_{ems} pulls i_{source} in phase with v_{source}. This system response is illustrated in Figure 3. Observe that the amplitude of i_{ems} increases over 0.30 s until i_{ems} reaches steady-state operation, indicating that a unity power factor is achieved at the grid.

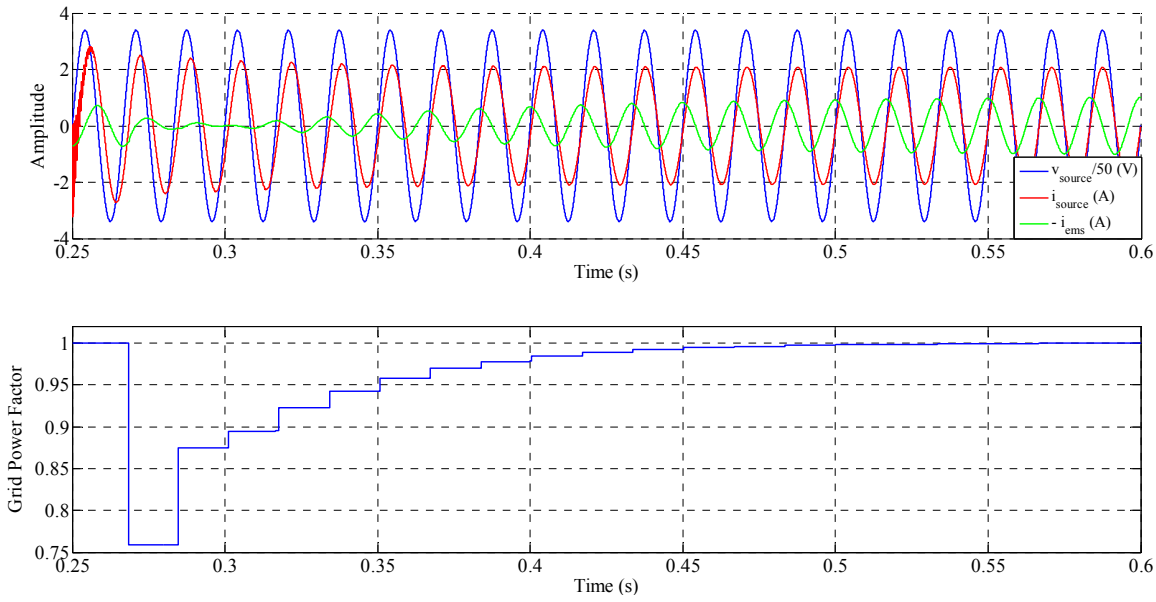

Figure 3. Grid power factor improvement for the 0.246 H load case.

It is important to note that $-i_{ems}$ is displayed in Figures 3 to satisfy the passive sign convention. The passive sign convention dictates that the reference direction for positive current flow is into a load; however, the simulation treats the EMS as a source whereby i_{ems} flows out of the EMS as shown in Figure 2. Hence, $-i_{ems}$ is presented in the results to show the positive flow of current into the EMS, which is consistent with the reference direction used to describe the positive flow of current to all other loads.

To validate the simulation results, an experiment was conducted for the same load scenario. The EMS was encoded to run the Simulink program, and the ohmic-inductive load was placed on the EMS to replicate the aforementioned simulation scenario. The results of the experiment are shown in Figures 4 and 5.

The EMS was not turned on at the start of the experiment so that the effects of the inductive power demand on the grid could be observed. Note in Figure 4 that the ohmic-inductive load creates a lagging power factor at the grid since i_{source} lags v_{source} by approximately 30°, which translates into an 87% source power factor. The power factor inconsistency between the two trials is expected since the simulation neglects the many electronic devices that induce reactance within the circuit..

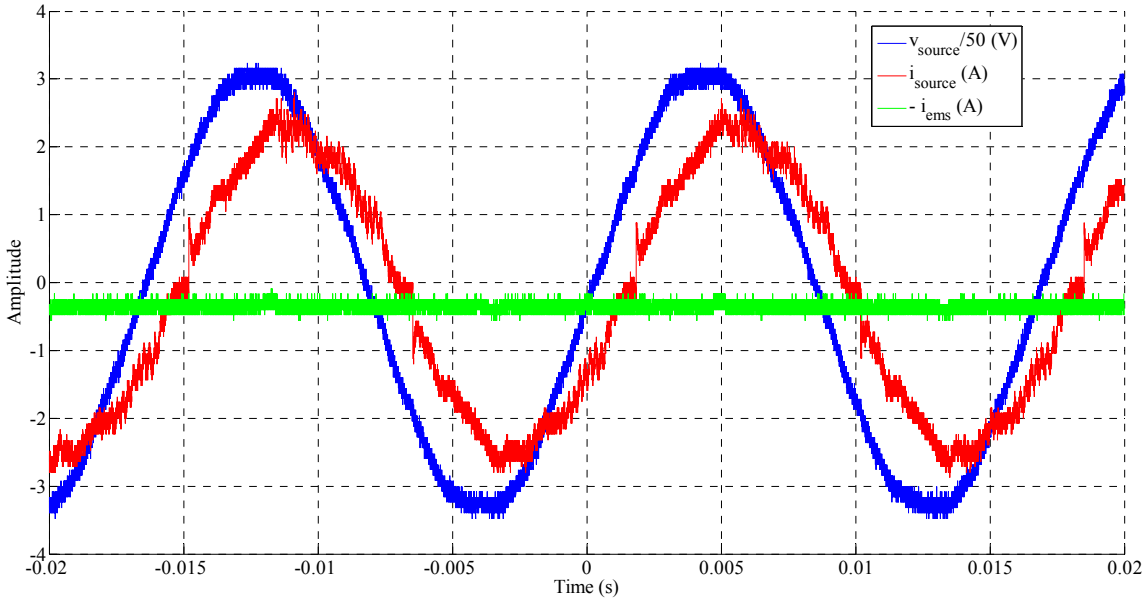

Figure 4. Source voltage and current when EMS current is off.

Once the EMS is turned on, capacitive power is delivered to the system via a leading i_{ems}, causing the phase angle of i_{source} to slightly lead v_{source} as shown in Figure 5. This over-compensation of reactive power to the grid occurs because the EMS does not currently possess a sensor on the source current and is, therefore, incapable of conducting closed-loop current control of i_{ems} . The Simulink code commands the EMS to adjust the amplitude of injected i_{ems} until a unity power factor is achieved, but the EMS cannot adjust the amplitude of i_{ems} without the use of a proportional-integral (PI) controller. Hence, the EMS merely produces a steady 1.0 A peak (or A_{pk}) sinusoidal i_{ems} signal in quadrature with the source voltage, which forces the EMS to over-compensate in selling reactive power to the grid. Adding a source current sensor to the EMS is a planned hardware upgrade that should remedy the issue.

Observe in Figure 5 the obvious presence of harmonics in the i_{ems} signal. These harmonic signatures occur as a result of the PWM switching scheme used by the EMS to generate the i_{ems} signal. They are not evident in the simulation results since the circuit modeled in Simulink disregards the PWM associated with the EMS's power electronics.

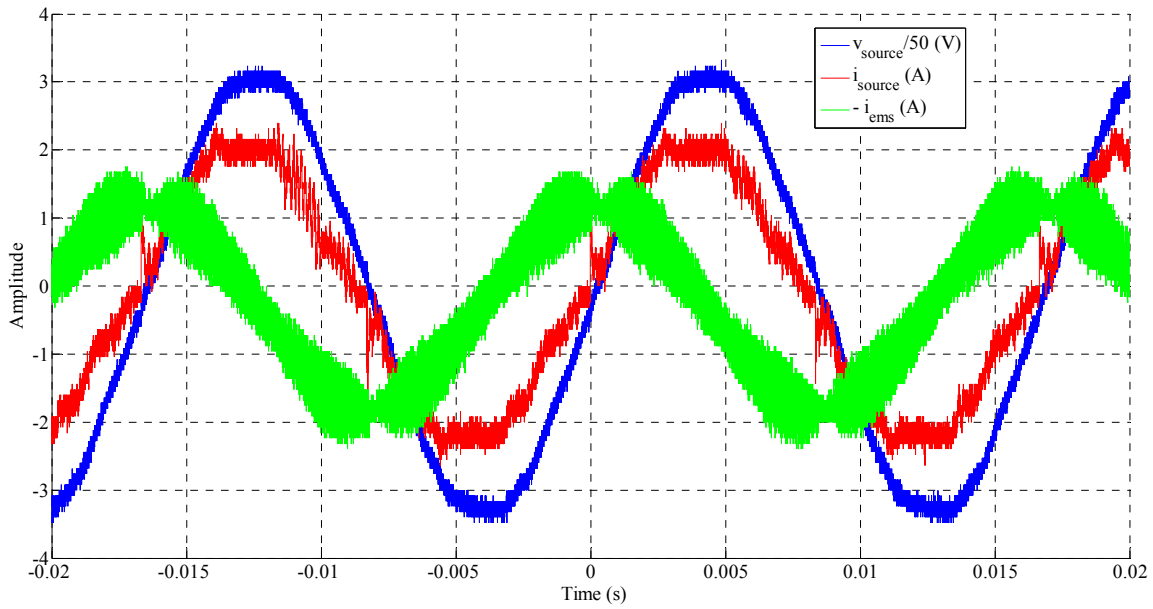

Figure 5. Source voltage and current when EMS current is on.

The ability of the EMS to operate as a current source in compensating for a reactive power demand on the grid was successfully demonstrated in this thesis. The method utilized a power factor improvement process developed in Simulink. Specifically, a zero-crossing detection algorithm tracked the power factor angle between the source voltage and current so that an appropriate amount of reactive current can be injected into the system at the PCC in order to achieve a unity power factor at the grid. The process was simulated to predict the system's response to capacitive and inductive power demands on the grid. A laboratory experiment was then conducted with the actual EMS to validate the process.

The results built confidence in the ability of the EMS to compensate for a reactive power demand on the grid; however, improving the simulation and experiment could potentially facilitate a better understanding of the EMS's capabilities. For example, the experiment should be repeated once a current sensor is added on the source. Also, the simulation could be further developed to model the EMS's power electronics architecture to include the PWM and controller required to operate the H-bridge inverter. Combining the two aforementioned efforts into a single project might provide for a better comparison of the simulation and experimental results.

ACKNOWLEDGMENTS

Much thanks to Professors Alex Julian and Giovanna Oriti for making this thesis a painless yet worthwhile experience.

THIS PAGE INTENTIONALLY LEFT BLANK

I. INTRODUCTION

A. BACKGROUND

The Department of Defense (DOD) has identified department-wide goals for increasing energy efficiency and reducing energy costs both on the battlefield and across its installations. In particular, the United States Marine Corps (USMC) and Department of the Navy (DON) seek to make 50% of all installations net-zero energy efficient and require that 50% of all energy consumption aboard installations come from alternative energy sources by 2020 [1]. These goals imply that the DON and USMC must pursue suitable energy management practices and technologies in addition to transitioning to alternative fuels in order to improve energy efficiency and reduce cost at installations.

A significant contributor to higher energy costs and reduced energy efficiency is the overall inductive power demand on the bulk electric grid by both DOD and civilian consumers. This inductive power demand reduces the power factor (PF) on the supply side of an electrically coupled power network, which creates numerous challenges to generating, transmitting, and distributing electric power to the consumer. These challenges are well-known and include voltage and power losses (reduced power efficiency) along transmission lines and in transformers, limited real (active) power supplied to the consumer, and higher energy and installation costs due to increased power rating requirements on generators and power distribution infrastructure necessary to support high reactive loads [2]. Transmission line length also affects cost since line losses vastly increase when power is transmitted over significant distances to the consumer [2]. This is often the case in California where power is commonly shipped from neighboring states. These costs are eventually passed on to the consumer. Along with ensuring energy security at installations [1], reducing energy costs is one of the foremost reasons why the DOD requires each net-zero energy installation to "produce as much energy on or near the installation as it consumes in its buildings and facilities" [3].

An example of reactive power costs charged directly to a commercial consumer in the UK is shown in Figure 1. Note that the installation was charged a fixed rate for a peak

load of 850 kVA. Real and reactive energy consumption was charged at assigned per unit rates; although, reactive power was charged at a much lower rate of 0.271 pence (0.45 cents) per kVARh (volt-ampere reactive hour). The installation's average power factor during the period was relatively high at 0.949 or 94.9% [2].

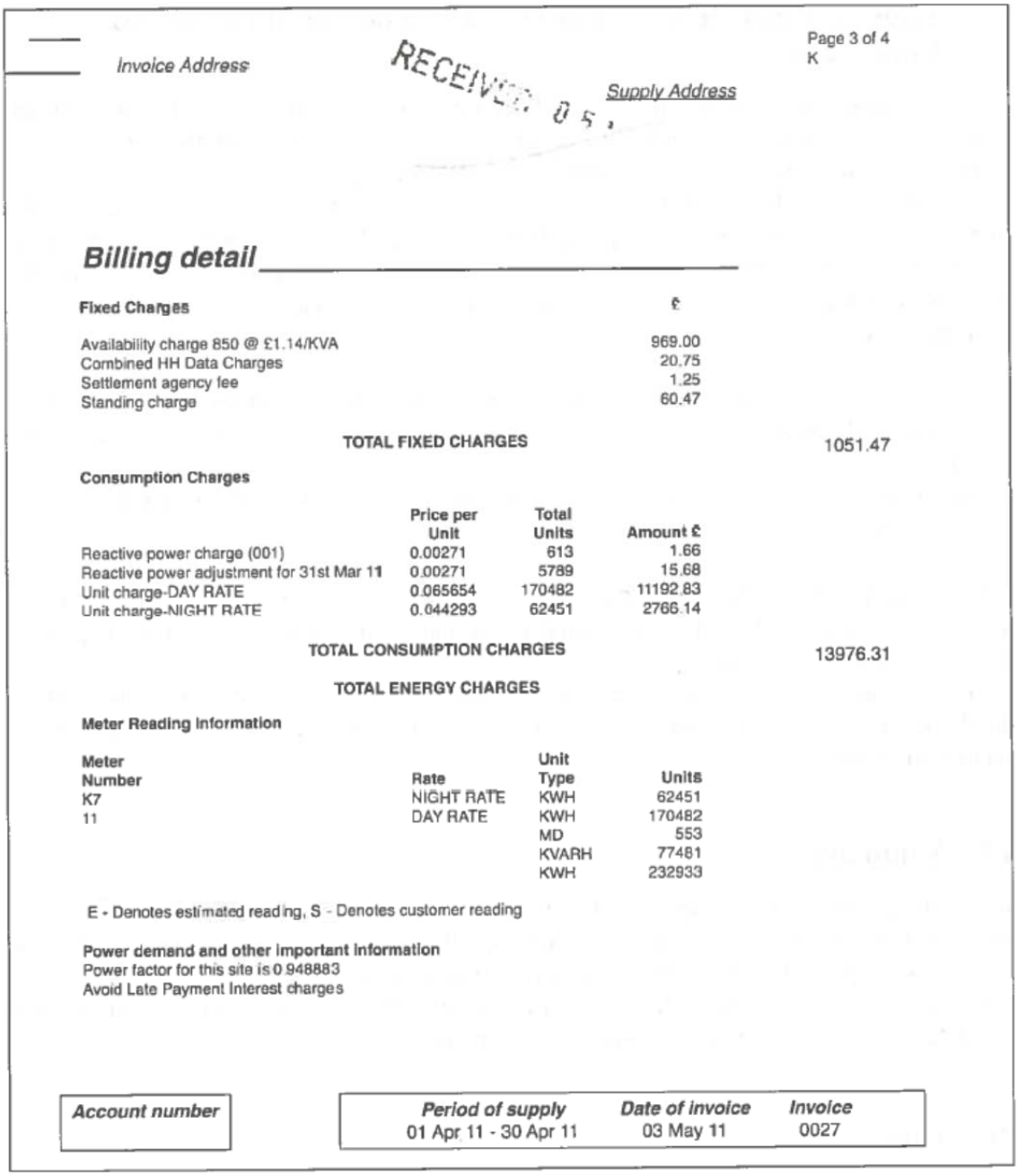

Invoice Address

RECEIVED 05

Supply Address

Page 3 of 4
K

Billing detail

Fixed Charges £

Availability charge 850 @ £1.14/KVA	969.00
Combined HH Data Charges	20.75
Settlement agency fee	1.25
Standing charge	60.47

TOTAL FIXED CHARGES 1051.47

Consumption Charges

	Price per Unit	Total Units	Amount £
Reactive power charge (001)	0.00271	613	1.66
Reactive power adjustment for 31st Mar 11	0.00271	5789	15.68
Unit charge-DAY RATE	0.065654	170482	11192.83
Unit charge-NIGHT RATE	0.044293	62451	2766.14

TOTAL CONSUMPTION CHARGES 13976.31

TOTAL ENERGY CHARGES

Meter Reading Information

Meter Number	Rate	Unit Type	Units
K7	NIGHT RATE	KWH	62451
11	DAY RATE	KWH	170482
		MD	553
		KVARH	77481
		KWH	232933

E - Denotes estimated reading, S - Denotes customer reading

Power demand and other important information
Power factor for this site is 0.948883
Avoid Late Payment Interest charges

Account number	Period of supply	Date of invoice	Invoice
	01 Apr 11 - 30 Apr 11	03 May 11	0027

Figure 1. UK power bill, from [2].

Commercial consumers in the United States typically are not charged directly for reactive power consumption. Instead, they are charged for their real power usage at higher peak and off-peak rates than in the UK and assessed a rebate for reactive power savings resulting from a high average power factor during the billing cycle. This practice is demonstrated by the Pacific Gas and Electric (PG&E) power bill for Naval Postgraduate School (NPS) in Monterey, California, shown in Figure 2. Note that NPS received a $458.21 rebate based on a power factor of 0.93 or 93%. The bill is split into two parts due to a utility rate change that occurred during the billing period.

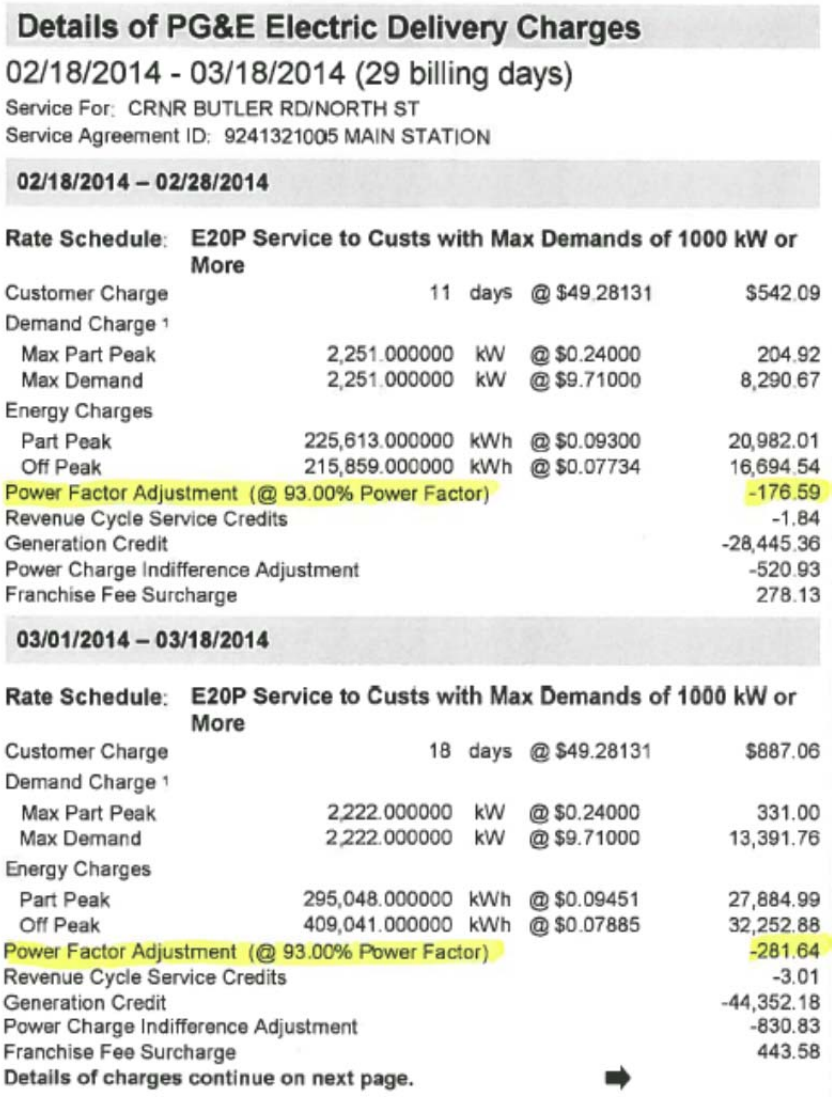

Details of PG&E Electric Delivery Charges

02/18/2014 - 03/18/2014 (29 billing days)

Service For: CRNR BUTLER RD/NORTH ST
Service Agreement ID: 9241321005 MAIN STATION

02/18/2014 – 02/28/2014

Rate Schedule:	**E20P Service to Custs with Max Demands of 1000 kW or More**			
Customer Charge	11	days	@ $49.28131	$542.09
Demand Charge 1				
Max Part Peak	2,251.000000	kW	@ $0.24000	204.92
Max Demand	2,251.000000	kW	@ $9.71000	8,290.67
Energy Charges				
Part Peak	225,613.000000	kWh	@ $0.09300	20,982.01
Off Peak	215,859.000000	kWh	@ $0.07734	16,694.54
Power Factor Adjustment (@ 93.00% Power Factor)				-176.59
Revenue Cycle Service Credits				-1.84
Generation Credit				-28,445.36
Power Charge Indifference Adjustment				-520.93
Franchise Fee Surcharge				278.13

03/01/2014 – 03/18/2014

Rate Schedule:	**E20P Service to Custs with Max Demands of 1000 kW or More**			
Customer Charge	18	days	@ $49.28131	$887.06
Demand Charge 1				
Max Part Peak	2,222.000000	kW	@ $0.24000	331.00
Max Demand	2,222.000000	kW	@ $9.71000	13,391.76
Energy Charges				
Part Peak	295,048.000000	kWh	@ $0.09451	27,884.99
Off Peak	409,041.000000	kWh	@ $0.07885	32,252.88
Power Factor Adjustment (@ 93.00% Power Factor)				-281.64
Revenue Cycle Service Credits				-3.01
Generation Credit				-44,352.18
Power Charge Indifference Adjustment				-830.83
Franchise Fee Surcharge				443.58

Details of charges continue on next page.

Figure 2. PG&E power bill for NPS.

From a comparison of Figures 1 and 2, it is apparent that energy cost savings can be achieved by compensating for reactive power, which directly relates to power factor improvement. The power factor is a measure of power efficiency and, therefore, plays an important role in understanding reactive power compensation. The power factor describes how efficiently a supply delivers real power to a load and is mathematically defined as

$$PF = \cos(\varphi) \tag{1}$$

where the power factor angle $\varphi = \theta_v - \theta_i$ is the difference between the voltage and current phase angles. A unity power factor (i.e., $PF = 1$) implies that a sinusoidal voltage and current are in phase (i.e., $\theta_v = \theta_i$), which yields maximum real power flow since the relationship between power factor and real power P is given by

$$P = V \cdot I \cdot \cos(\theta_v - \theta_i) \tag{2}$$

where voltage V and current I are the root mean square (RMS) values of the voltage and current. Conversely, a unity power factor implies no reactive power flow since reactive power Q is given by

$$Q = V \cdot I \cdot \sin(\theta_v - \theta_i). \tag{3}$$

Hence, achieving a unity power factor at a desired location in a circuit is the objective in reducing reactive power flow at the same point.

In addition to creating energy cost savings, reactive power compensation increases energy efficiency gains. As previously discussed, transmission lines bleed reactive power more quickly than real power, which increases power losses and reduces power efficiency along the transmission lines—especially over long distances [4]. Also, most consumer loads are inductive in nature. The current of an inductance lags the voltage resulting in a lagging power factor, which tends to lower the system voltage [4] by drawing reactive energy from the system. As such, inductive loads typically cause voltage sags along transmission lines that limit the delivery of real power to the consumer. Conversely, the current of a capacitance leads the voltage resulting in a leading power factor, which tends to raise the system voltage [4] by delivering reactive energy to the system. Providing capacitive power support to the power distribution system, therefore, reduces power losses and improves voltage quality along transmission

lines [4]. Transmitting reactive power also increases the amount of RMS current in the transmission lines, which results in additional line losses since $P_{loss} = I^2 R$. Hence, reducing reactive power demand likewise enhances the delivery of real power to the consumer since current otherwise wasted in power loss or transmitting reactive power is used to transmit real power.

The compensation of reactive power ideally occurs as close to the inductive load as possible in order to eliminate the need for reactive power support from the grid by achieving a unity power factor [2]. This typically happens at the point of common coupling (PCC) in an electrically coupled distribution network. By providing compensating reactive power at the PCC, power lines from the supplier to the consumer are loaded only with active energy supplied by the grid [2]. Compensating to a less-than-unity power factor requires additional reactive power support from the grid, which further burdens feed-in lines to the consumer and reduces energy efficiency as a result of energy losses in transmission [2].

There are many common ways to compensate for inductive power. Most of these are not discussed in this thesis; however, the use of an energy management system (EMS) to control reactive power in a system is investigated. EMS applications in power electronics are becoming increasingly popular. An EMS can monitor reactive power requirements in an electrical circuit and inject reactive power when and where necessary in a circuit to increase energy efficiency within a system or limit the reactive power supply burden on the bulk electric grid and distributed generation (DG) sources. The EMS investigated in this thesis is described in more detail in the next chapter.

B. OBJECTIVE

The purpose of this thesis is to demonstrate the capability of an EMS to compensate for a reactive power demand on the grid. This is accomplished by first using zero-crossing detection to determine the source power factor angle φ_{source} between the source voltage and current. The appropriate amount of reactive power is then injected into the system using the EMS as a reactive current source in order to achieve a unity power factor at the grid. Although the power factor improvement of a single-phase grid is

investigated in this thesis, the EMS can provide the same capability to three-phase systems.

C. APPROACH

In order to adequately demonstrate the ability of the EMS to facilitate reactive power compensation and achieve a unity power factor at the source, the first step was to model the EMS with zero-crossing detection capability and closed-loop current control using Simulink software [5]. Varying loads were scheduled in the simulation to show the capability of the EMS to compensate for a changing reactive power demand on the grid. The Simulink model was streamlined in order to better isolate the zero-crossing detection feature of the EMS for the purpose of simplifying data collection and analysis. Certain model subsystems deemed unnecessary or extraneous for the purpose of this thesis were removed.

Finally, a laboratory experiment was conducted using the EMS. The Simulink model was compiled into code that commanded the EMS to operate as a current source in compensating reactive power using zero-crossing detection. Experimental data was collected and compared to the simulation results.

D. PREVIOUS WORK

Much research involving the EMS discussed in this paper has been conducted to date. Previous Naval Postgraduate School students have added capabilities to the EMS over the years thereby evolving it into the current system. Recent work includes designing the EMS to choose between two different generators and a battery bank to power loads typically found at a forward operating base with the goal of improving fuel efficiency [6]. The ability of the EMS to store unused energy in the battery bank and disable generator power during periods of light loading [6] is also demonstrated. Other works include an analysis of the effects on microgrid power quality given different H-bridge inverter loading schemes [7] and using the EMS to manage peak power demand on a microgrid in order to improve energy efficiency and reduce energy costs [8].

While the addition of a reactive power compensation capability to the EMS is discussed in this thesis, reactive power compensation using energy management systems is not a new concept. In one particular IEEE Industry Applications Magazine article, the authors investigate via simulation the addition of decision-making ability to a multifunctional single-phase voltage-source inverter (VSI) [9]. The inverter possesses the same smart functionalities as the EMS studied in this thesis. Specifically, the authors demonstrate the VSI's ability to select from various modes of operation in response to certain system conditions or electricity pricing.

In one particular case, the inverter detects a voltage sag at the grid, which is created by the reactive power demand of two VSI loads. The inverter then schedules reactive power to the PCC to alleviate the voltage sag [9]. The result is shown in Figure 3. Note that the voltage sag is created at 0.5 s. The inverter immediately compensates, and the voltage sag is corrected after 1.2 s. However, the inverter continues to sell reactive power to the grid, causing a spike in grid voltage. The inverter's static synchronous compensator function then absorbs the excess reactive power causing the grid voltage to stabilize [9].

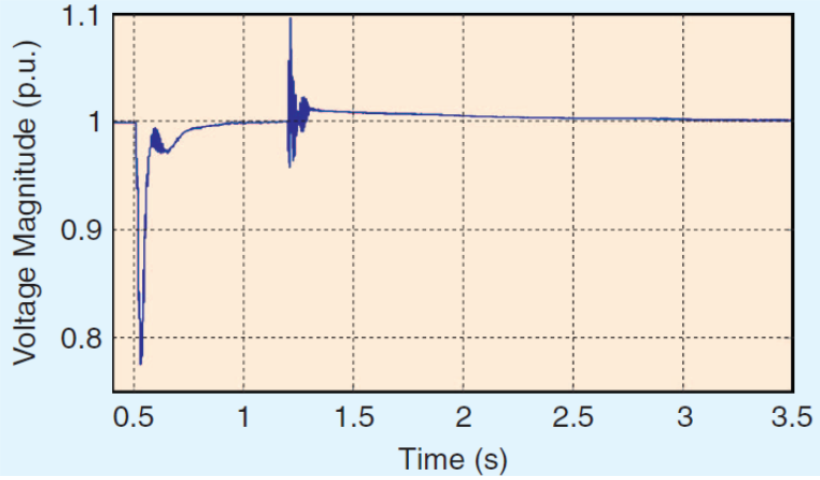

Figure 3. Per unit grid voltage magnitude, from [9].

In another paper, the authors demonstrate closed-loop current control in utilizing DG unit "interfacing converters to actively compensate harmonics" [10]. A cost-effective

solution whereby fundamental and harmonic DG currents are independently controlled without the need for current detection in the load or voltage detection in the distribution system is proposed [10]. The authors also use a simple closed-loop power control method to detect the fundamental current reference without the use of phase-locked loops thereby avoiding fundamental current tracking errors [10]. A similar closed-loop control facilitating reactive power control is later demonstrated in this thesis.

II. ENERGY MANAGEMENT SYSTEM

A. FUNCTIONALITY

The EMS utilized in this thesis is designed as an enabling technology capable of providing digitally-controlled "smart grid" functionality to electrical power consumers by facilitating power flow control to the consumer while simultaneously increasing power reliability and improving energy system security [11]. Depending on the situation, the EMS can act as a voltage source or a current source either while connected to a main AC source such as a bulk power grid or independent of the grid in islanded mode using various DG sources (photovoltaic panels, fuel cells, gas generators, batteries, etc.). Moreover, the EMS possesses an energy storage capability currently in the form of a lead-acid battery bank [11]. The following list details the major functions of the EMS [11]:

- User interfacing to facilitate selective functionality.
- Real and reactive power tracking and control.
- Peak power management.
- Power quality control and reliability enhancement.
- Load scheduling and management to include non-critical load shedding and critical load maintenance.
- Source power management to include DG source application.
- Energy storage management.
- Fault detection and correction.

A block diagram demonstrating how the EMS might interface with its environment is provided in Figure 4. Note that the EMS integrates DG sources and storage capabilities to support various loads based on priorities established by the consumer. Ideally, the EMS provides power support to the grid unless a specified power management scenario calls for autonomous operation as previously discussed.

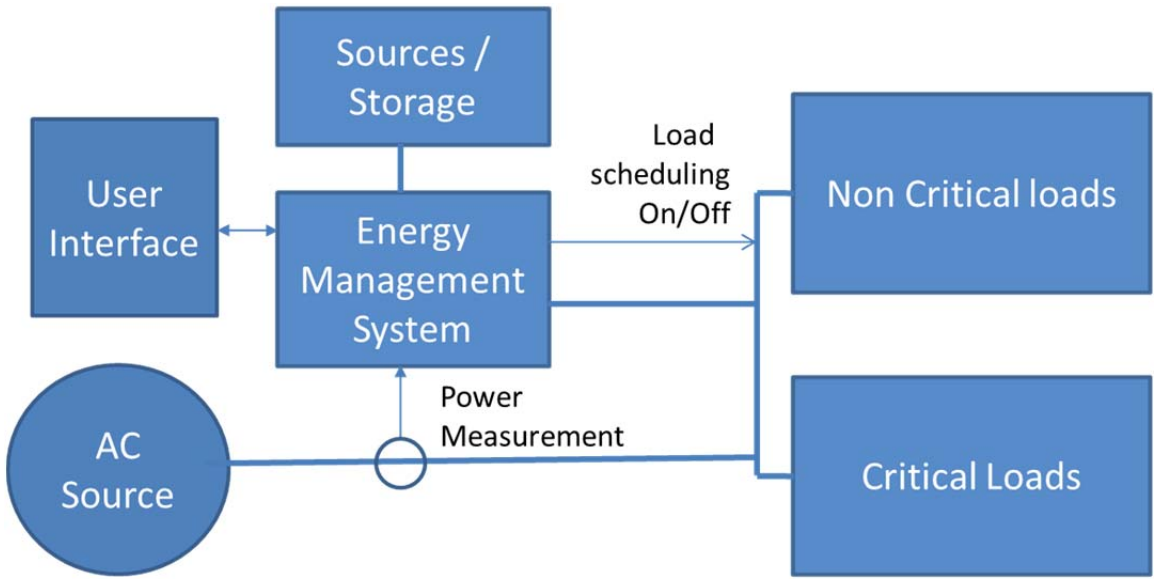

Figure 4. EMS interfacing with its environment, from [11].

B. HARDWARE OVERVIEW

A photograph of the EMS discussed in this paper is shown in Figure 5. Note that the EMS consists of power electronics framed on upper and lower printed circuit boards (PCB) with input/output ports and a processor cooling system. The EMS hardware is represented by the block diagram shown in Figure 6 and adequately explained in [11].

The EMS's power electronics interface with various inputs located to the right of the PCB is illustrated in Figure 6. The field programmable gate array (FPGA) development board communicates with a personal computer (PC) via an interface chip. The interface chip and PC couple via a joint test action group (JTAG) connector. Simulink code from the PC is compiled to VHDL code using Xilinx System Generator software [12], which is used by the FPGA to command the EMS. The FPGA development board is the middle board shown in Figure 5. The integrated power module (IPM), DC power supply, passive filters, and voltage and current sensors reside on the lower PCB. The IPM contains insulated gate bipolar transistor (IGBT) gate drive circuitry in three-phase configuration, which facilitates power flow control between the grid, DG sources, battery bank, and assigned loads. The voltage and current sensors interface with the FPGA development board via a series of analog-to-digital converters

located on the upper PCB. Also located on the upper PCB is a transistor-to-transistor interface used to command power from assigned DG sources and manage various loads. Finally, an LCD shows desired feedback information to the user.

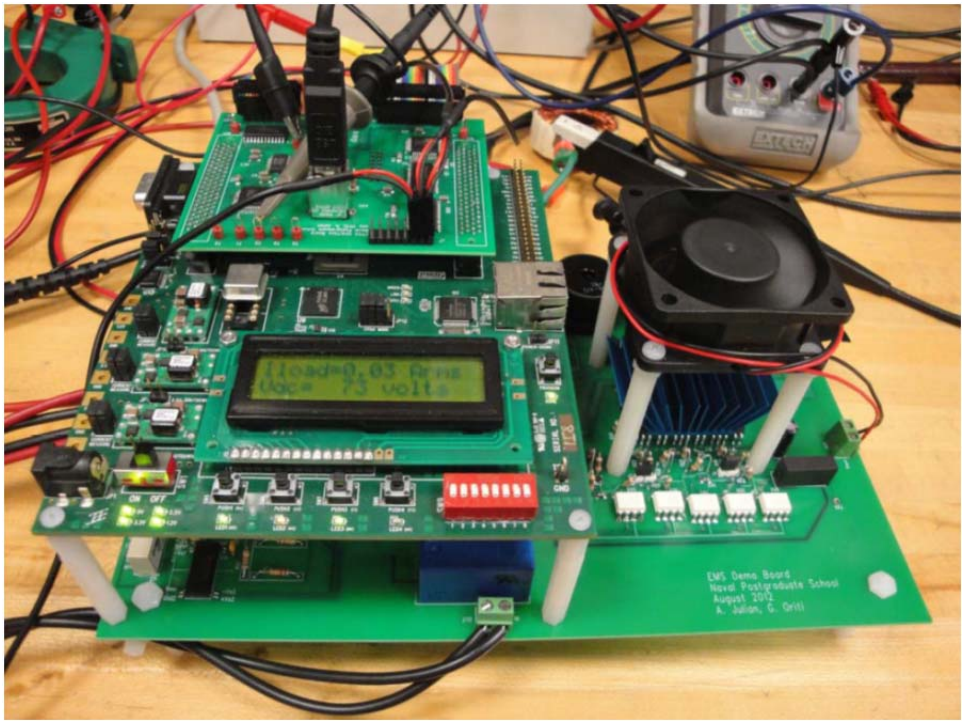

Figure 5. Photograph of the EMS analyzed in this thesis.

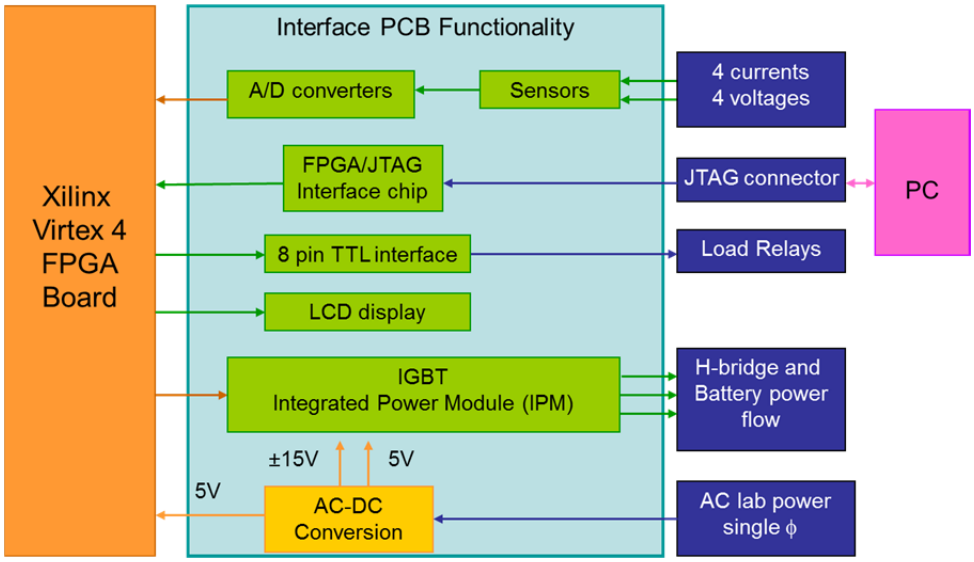

Figure 6. EMS interfacing diagram.

C. MODELING APPROACH

As previously discussed, the objective of this paper is to demonstrate the capability of the EMS to compensate for a reactive power demand on the source by injecting the appropriate amount of compensating reactive current into the system at the PCC. This capability is described in detail in the following chapter; however, it is important to understand the method for modeling this process in this thesis and how it differs from actual EMS functionality.

A schematic demonstrating the means by which the IPM interfaces critical and non-critical loads with AC and DC power supplies is provided in Figure 7. The EMS uses a single-phase H-bridge inverter consisting of two single-leg inverters, which is preferred over other inverter types in high power applications [13]. A third leg connects a DC power supply to the H-bridge inverter via a buck-boost DC-to-DC converter. A pulse width modulation (PWM) scheme with unipolar voltage switching delivers the H-bridge gate signals [7] and reduces the effects of harmonics in the output voltage at the switching frequency [13]. A low-pass LC filter (LPF) facilitates a clean AC signal at the output of the inverter. The LPF is shown in Figure 7. Note that the filter capacitor is marked by v_{ac}, and reactive current i_{ems} flows through the filter inductor.

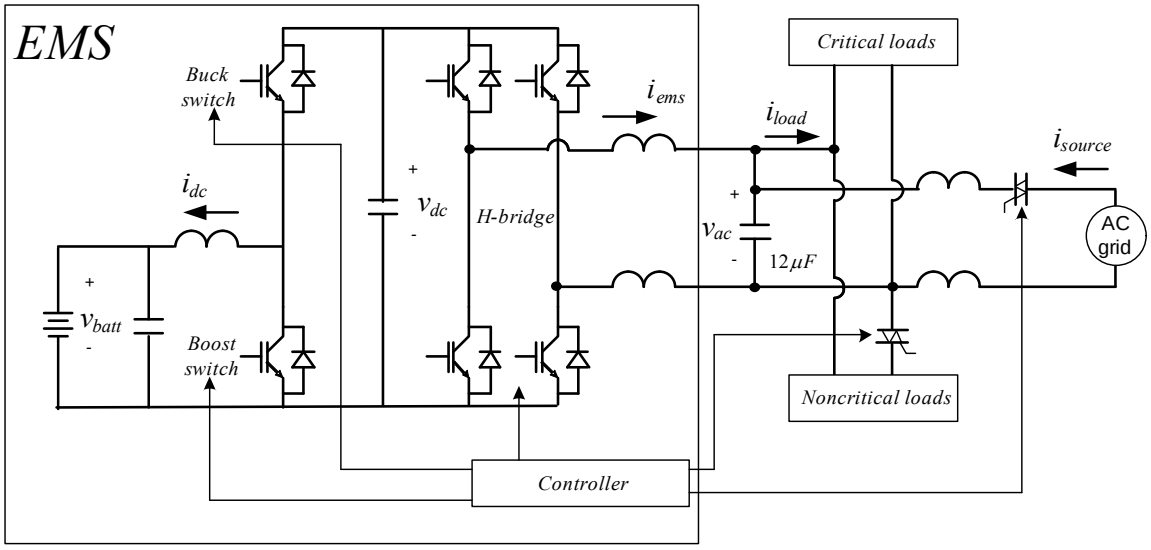

Figure 7. EMS power electronics circuit schematic.

Recall that the H-bridge inverter can be controlled as a current source or a voltage source. For the purpose of this thesis, the H-bridge inverter is controlled as a current source using a programmable microcontroller. The microcontroller provides a number of control features to the EMS. In particular, it regulates the polarity of the output voltage from the H-bridge inverter by controlling the H-bridge inverter's IGBT switches and controls the flow of power using feedback provided by a sensor positioned at the load. This control scheme is shown in Figure 7.

As a current source, the EMS produces an output current i_{ems}, which is used to inject compensating reactive power at the PCC. A particular method for controlling i_{ems} in providing reactive power support to the AC grid is demonstrated in this thesis. This method involves using a Simulink-based zero-crossing detection algorithm to determine the power factor angle φ_{source} at the grid and, subsequently, changing the amplitude of the compensating reactive current i_{ems} to bring φ_{source} to zero. Achieving a unity power factor at the source eliminates reactive power demand on the grid.

To effectively model this process, an equivalent of the circuit shown in Figure 7 is simulated using Simulink software. The reason for using an equivalent circuit is to demonstrate the EMS as a constant current source in order to examine the use of i_{ems} in compensating for a reactive power demand on the AC grid. A schematic of the idealized circuit is illustrated in Figure 8. Modeling the EMS in this fashion assumes a clean sinusoidal i_{ems} signal from the H-bridge inverter without having to consider pulse width modulation and associated closed-loop voltage control to produce the i_{ems} necessary to achieve a unity power factor at the grid.

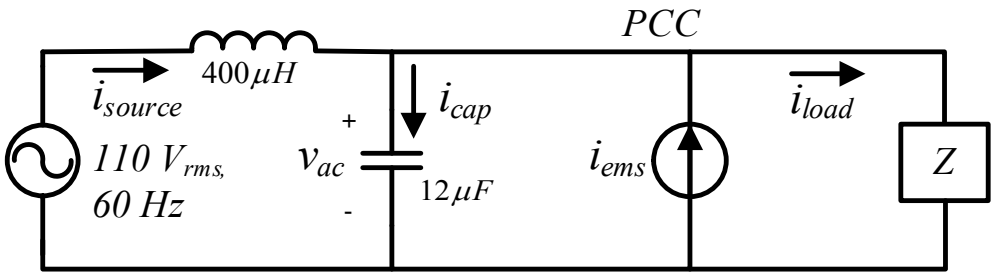

Figure 8. Idealized circuit schematic.

Notice from Figure 8 that the EMS block in Figure 7 is effectively eliminated from the idealized circuit. All circuitry to the left of the 12 μF filter capacitor in Figure 7 is not considered in the schematic in Figure 8 except for the flow of i_{ems} from the EMS to the PCC. This idealized modeling scheme facilitates a more focused examination of the power factor improvement methodology developed for the EMS using Simulink, which is explained in detail in Chapter III.

The experimental EMS of course remains as shown in Figure 7 and, therefore, employs pulse width modulation to create the H-bridge gate signals that generate a voltage to control i_{ems}. The power factor improvement methodology developed in Simulink still applies to the experiment, but no proportional-integral (PI) controller was implemented in the lab to correct i_{ems} because the EMS hardware currently does not have a sensor on the source current. Adding a sensor to the source current is a planned upgrade to the system. Due to this restraint, the experiment was conducted without the use of closed-loop current control, but the EMS still demonstrated the capability to generate compensating reactive current in response to a reactive power demand on the grid. The results are explained in further detail in Chapter IV.

III. COMPUTER SIMULATION

A. OVERVIEW

A computer simulation of the idealized circuit shown in Figure 8 was created using Simulink. The simulation design is based on the circuit shown in Figure 9, which is the same circuit presented in Figure 8 except with two defined variable loads tested both in simulation and experiment. Load 1 is a purely resistive 85.7 Ω load. Load 2 is a 0.246 H inductive load with an estimated internal resistance of 5 Ω. The purpose of the two loads is to demonstrate the capability of the EMS to compensate for a varying reactive power demand on the grid.

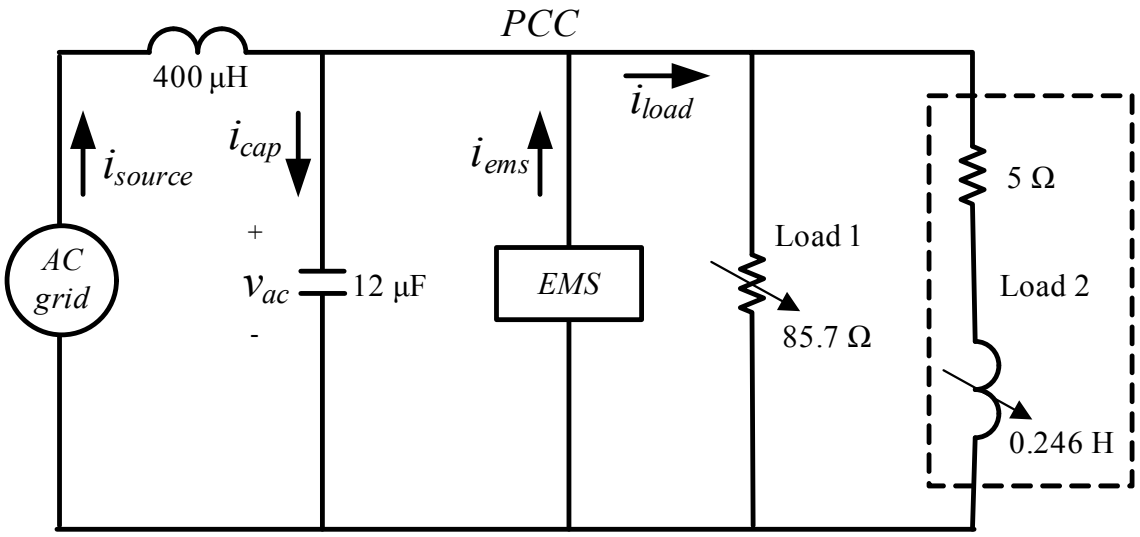

Figure 9. Circuit schematic replicated in simulation.

The circuit is mathematically simulated by the circuit component and subsystem diagram in Figure 10. The 12 µF filter capacitor and 400 µH filter inductor with 10 mΩ resistance are clearly displayed in the diagram as independent of the subsystems. A constant 110 V_{rms}, 60 Hz sinusoidal input signal from the grid precedes the filter inductor. The *Load Switching* subsystem contains both variable loads, which are controlled by an electronic switch that adds inductance to the system at a predetermined time in the simulation. The *Power Factor Correction* subsystem contains the zero-crossing detection

and power factor angle error correction algorithms used to continuously track phase angles of v_{source} and i_{source} ($\theta_{v_{source}}$ and $\theta_{i_{source}}$, respectively) and subsequently determine and correct power factor angle φ_{source} in order to achieve a unity power factor at the grid. The *Power Factor Correction* subsystem also employs closed-loop current control, which drives φ_{source} to zero by changing the amplitude of i_{ems} as it flows to the PCC.

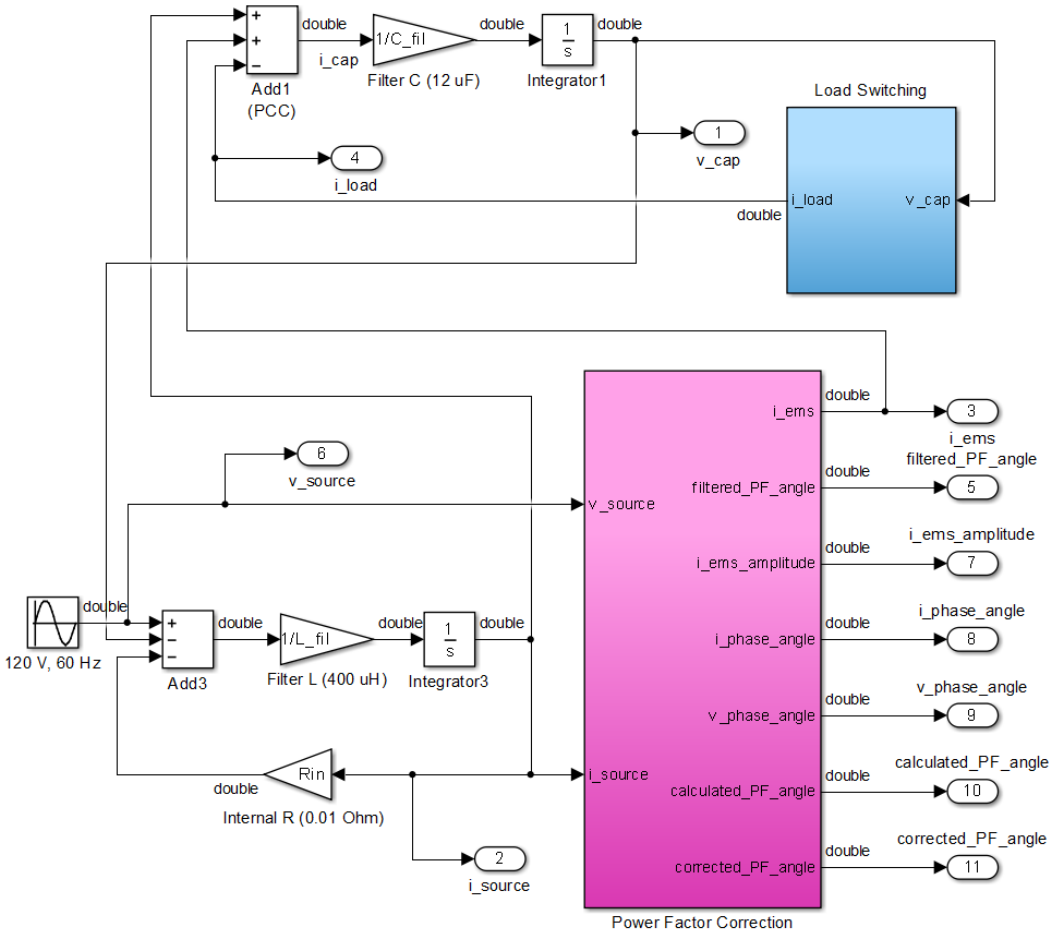

Figure 10. Simulink circuit component and subsystem diagram.

To keep the model as visually clean as possible, all circuit data regarding output variables 1 through 11 (depicted in Figure 10) is sent to the top-level block diagram shown in Figure 11. There it is collected along with simulation time and sent to the MATLAB "workspace" for graphical analysis. The MATLAB file scripts containing the

system's initial conditions, discrete component values, and code used to create the plots in this thesis are presented in the Appendix.

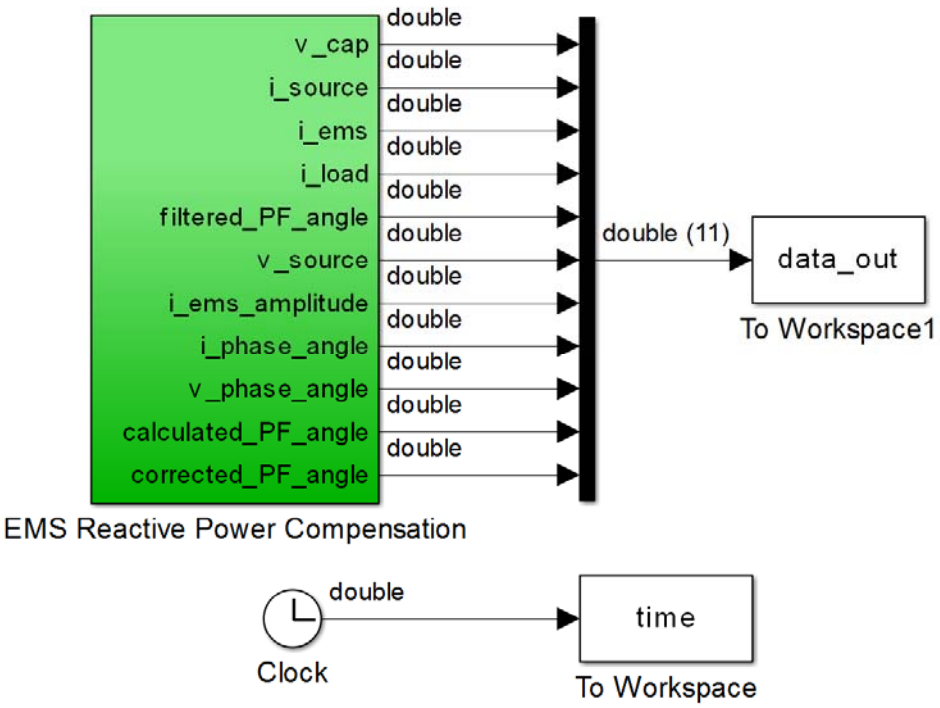

Figure 11. Simulink top-level block diagram.

B. LOAD SWITCHING

As previously stated, load switching is used to demonstrate the capability of the EMS to compensate for a varying reactive power demand on the grid. The resistive and inductive loads shown in Figure 9 are simulated using the load switching subsystem presented in Figure 12. At the start of the simulation, only the 85.7 Ω load is active, which results in an overall capacitive reactance in the circuit due to the dominating presence of the 12 μF low-pass filter capacitor in the circuit. The result is an overall capacitive power demand on the source that is quickly compensated by the injection of inductive i_{ems} at the PCC.

At 0.25 s into the simulation, the 0.246 H inductive load with 5 Ω internal resistance is added to the circuit. The load switching operation is controlled by the *load*

step and *Switch1* function blocks shown in Figure 12. This new load scheme creates an overall inductive power demand on the grid that models the power demand of a typical reactive power consumer. A capacitive i_{ems} is accordingly injected at the PCC to correct the lagging power factor produced at the grid by the inductive load. The results are presented in Section D of this chapter.

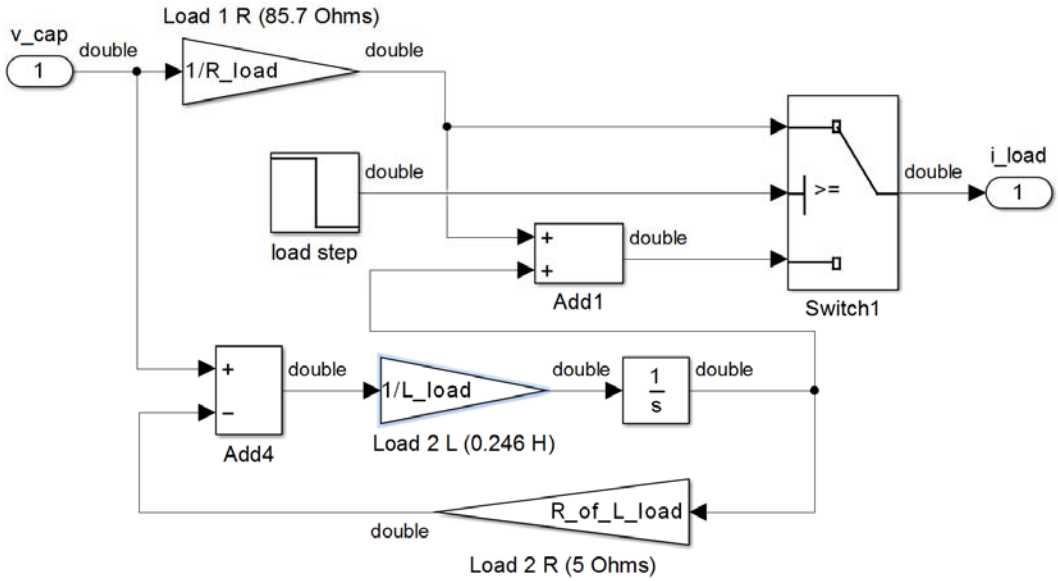

Figure 12. Simulink load switching subsystem diagram.

C. POWER FACTOR CORRECTION

The method used to create a unity power factor at the source is conceptually simple. The power factor correction flow chart shown in Figure 13 illustrates the process. First, the source power factor angle φ_{source} is calculated using zero-crossing detection. As φ_{source} is gradually driven to zero via closed-loop control, it is passed through a simple first-order, low-pass filter transfer function. The LPF filter softens the change in φ_{source} over time, which assists the PI controller in smoothly adjusting reference current amplitude I^*_{ems}. The EMS concurrently generates a continuous 1.0 A_{pk} sinusoidal current in quadrature with the sinusoidal source voltage that is multiplied with I^*_{ems} to create the sinusoidal EMS reference current i^*_{ems}. The reference current i^*_{ems} is designed to lead

v_{source} by 90° when i_{source} lags v_{source} so that i^*_{ems} improves the power factor at the grid when injected into the system. Alternatively, the reference current amplitude I^*_{ems} will be negative so that the injected i^*_{ems} lags v_{source} by 90° in order to improve a leading grid power factor.

Conceptually, i^*_{ems} is then compared to the measured EMS output current i_{ems} per the flow chart. The difference between the two waveforms defines the error that is corrected by another PI controller, which directs the inverter to generate a new i_{ems} via changes in the PWM scheme until $i_{ems} = i^*_{ems}$. At this point, the system makes no further changes to i_{ems} since a unity power factor is realized at the grid. Recall that the experimental EMS currently lacks a sensor at the source, and it is not yet possible to use closed-loop control to makes changes to the actual PWM in the laboratory. The results of the experiment are discussed in Chapter IV.

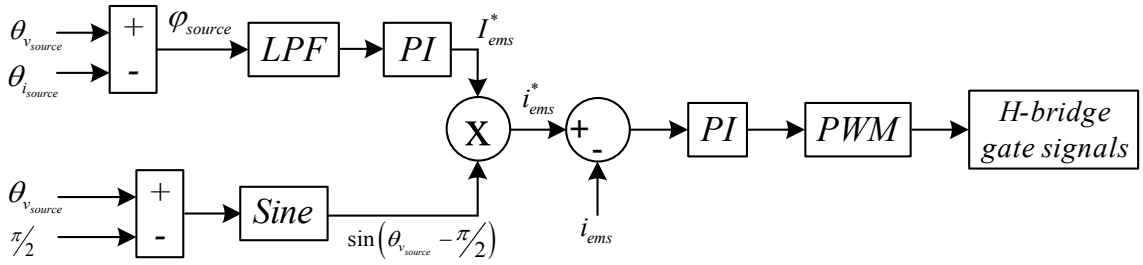

Figure 13. Power factor correction flow chart.

Recall from Figures 8 and 9 that the Simulink model does not account for PWM in the EMS and, therefore, does not create an i_{ems} signal. The simulation instead simplifies the power factor correction process by assuming that $i^*_{ems} = i_{ems}$ and, thus, only adjusts i^*_{ems} as necessary to correct the source power factor. Accordingly, i^*_{ems} feeds continuously into the PCC and is regulated via the first PI controller shown in Figure 13 as φ_{source} changes over time.

The function of the power factor correction diagram shown in Figure 14 is to implement the power factor correction flow chart in Figure 13 using Simulink. The components and subsystems that comprise the power factor correction block are illustrated by the Simulink power factor correction subsystem diagram in Figure 14. Note that the diagram replicates all flow chart functions leading to the creation of the i^*_{ems} signal. The PI controller and quadrature reference current signal are contained within the closed-loop current control subsystem. All parameter data is sent to the output of the power factor correction diagram to include i_{ems} , which is then injected back into the PCC as demonstrated in Figure 10.

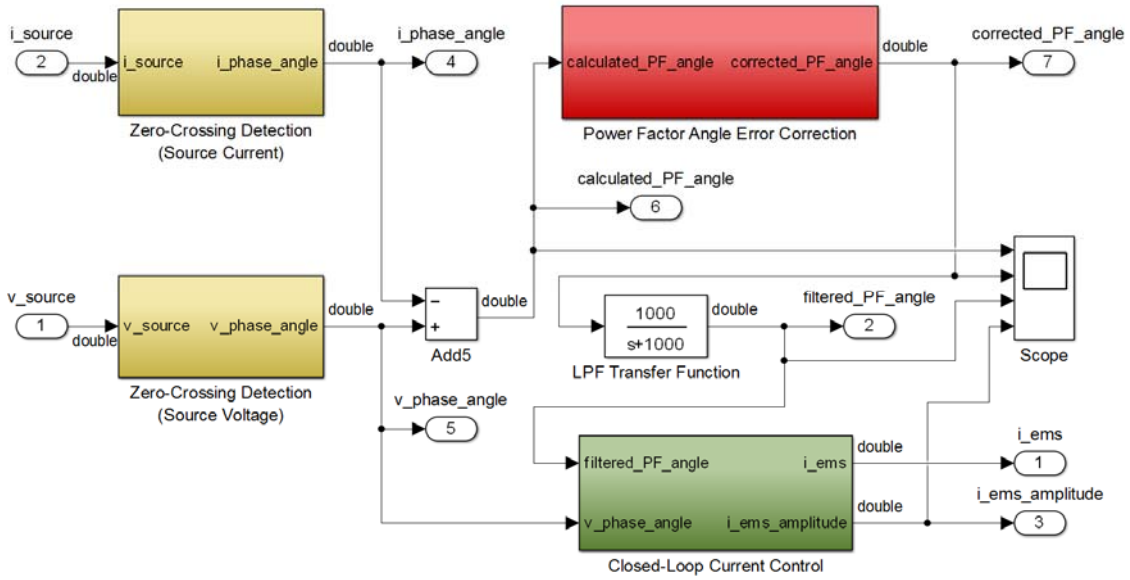

Figure 14. Simulink power factor correction subsystem diagram.

1. Zero-Crossing Detection

In order to determine the source power factor angle φ_{source}, the EMS uses zero-crossing detection algorithms to determine phase angles $\theta_{v_{source}}$ and $\theta_{i_{source}}$. These algorithms are located in the source voltage and source current *Zero-Crossing Detection* subsystems illustrated in Figure 14. The algorithm for determining $\theta_{v_{source}}$ is less complex

since v_{source} remains constant. The Simulink v_{source} zero-crossing detection algorithm for determining $\theta_{v_{source}}$ is shown in Figure 15.

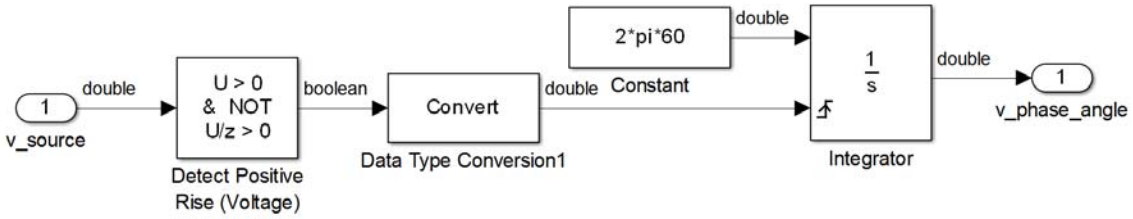

Figure 15. Simulink source voltage zero-crossing detection diagram.

The algorithm detects the positive rise of v_{source} by determining if the present sinusoidal voltage input value is positive and the previous value is non-positive. If a positive rise is detected, the *Detect Positive Rise* function block outputs a Boolean TRUE. Otherwise, the block outputs a Boolean FALSE. A TRUE statement signifies that the signal crossed the time axis while rising, which occurs once every cycle for a sinusoidal signal. The *Integrator* function block integrates over time t of the source voltage signal frequency from zero to a reset time of period T and then repeats. The integrator is programmed to reset when the *Detect Positive Rise* function block outputs a Boolean TRUE (i.e., detects a positive rise across the time axis). The result gives the phase angle by the relationship

$$\theta = \int_0^T 2\pi f dt \tag{4}$$

where the period T is the time between successive positive rises across the time axis and f is the signal frequency, which is typically 60 Hz for the grid voltage.

The EMS computes $\theta_{i_{source}}$ using an algorithm similar to that of $\theta_{v_{source}}$ except the i_{source} zero-crossing detection algorithm compares each integrator output value of $\theta_{i_{source}}$ to the quantity 1.6π. The algorithm ensures that the present value of $\theta_{i_{source}}$ is greater than 1.6π during a positive rise before reporting a Boolean TRUE to the *Integrator* function block. This prevents the integrator from prematurely resetting in the event that signal

transients or disturbances in i_{source} cause the signal to unexpectedly perform a zero-crossing. This process is demonstrated by the Simulink diagram in Figure 16.

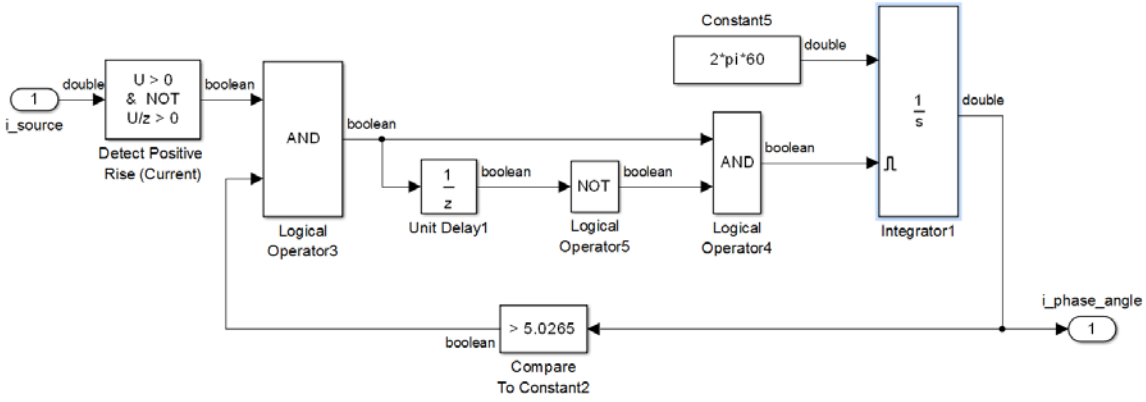

Figure 16. Simulink source current zero-crossing detection diagram.

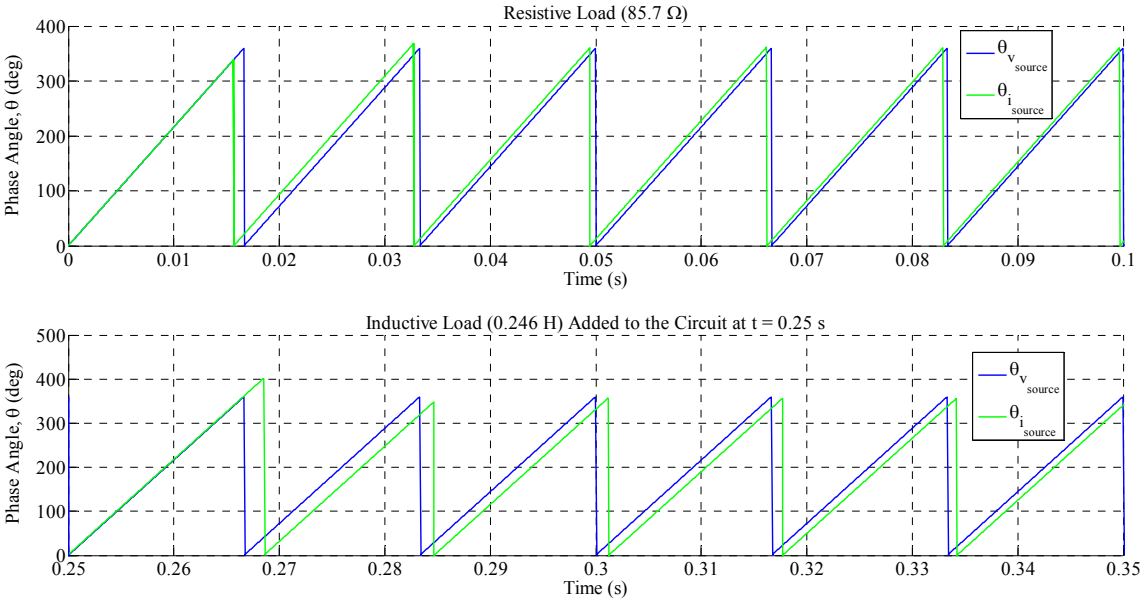

Figure 17. Source voltage and current phase angle plots for both load cases.

Plots showing the change in $\theta_{v_{source}}$ and $\theta_{i_{source}}$ over time for both the resistive and inductive load cases are presented in Figure 17. The graphic only shows the first 0.35 s of the simulation for the purpose of visual acuity. As previously mentioned, an overall capacitive reactance initially exists in the circuit before adding the inductive impedance to the load resulting in a leading power factor since i_{source} leads v_{source}. Once the inductive

load is introduced, the circuit experiences an overall inductive reactance, which causes i_{source} to lag v_{source} and results in a lagging power factor. Notice that the simulation gradually brings i_{source} in phase with v_{source} for both load cases since the simulation is running the power factor correction algorithm in the example.

2. Power Factor Angle Error Correction

The phase difference between $\theta_{v_{source}}$ and $\theta_{i_{source}}$ is then computed to determine the source power factor angle φ_{source} by subtracting the two quantities via the *Add5* block shown in the *Power Factor Correction* subsystem in Figure 14; however, computing φ_{source} in this fashion results in numerical errors. The errors are caused by the asynchronous resetting of the *Integrator* function blocks in Figures 15 and 16 in computing $\theta_{v_{source}}$ and $\theta_{i_{source}}$, respectively, using zero-crossing detection.

This mathematical glitch is best understood from Figure 17. In the inductive load case, for example, i_{source} lags v_{source} allowing the $\theta_{v_{source}}$ integrator to wrap from 2π to zero before the $\theta_{i_{source}}$ integrator. The result is a momentarily large φ_{source} that abruptly declines as φ_{source} approaches zero. These errors are displayed as spikes in the power factor calculation plot shown in Figure 18 and must be eliminated before closed-loop current control can operate to pull i_{source} in phase with v_{source}.

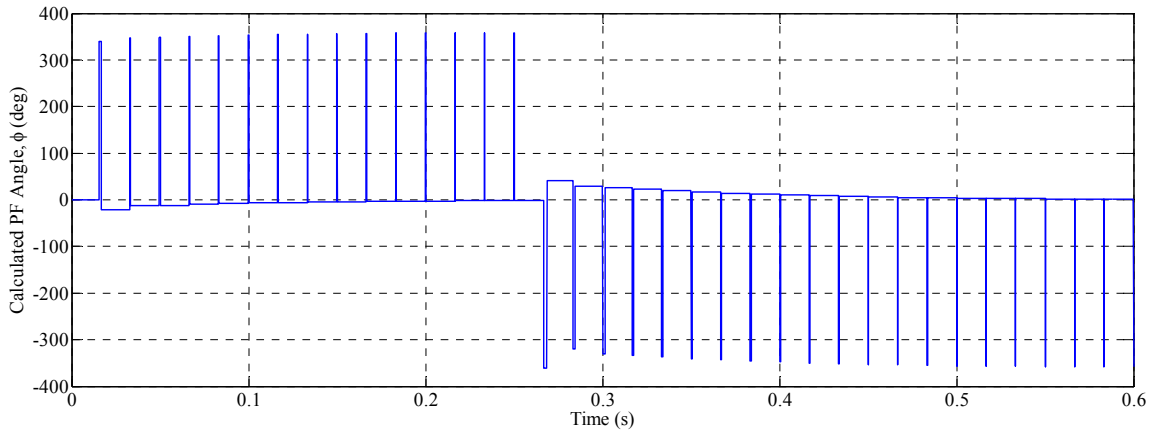

Figure 18. Power factor calculation with numerical integration error.

The *Power Factor Angle Error Correction* subsystem shown in Figure 19 eliminates the numerical error in φ_{source} simply by adding 2π to φ_{source} if φ_{source} is less than π or subtracting 2π from φ_{source} if φ_{source} is greater than π. This arithmetical process is possible since the calculated error in φ_{source} cannot be greater than ±2π simply because φ_{source} cannot mathematically be more than ±2π as demonstrated by the error spikes in Figure 18; hence, numerical error nears ±2π as φ_{source} approaches zero. Note in Figure 18 that the power factor angle is plotted in degrees instead of radians.

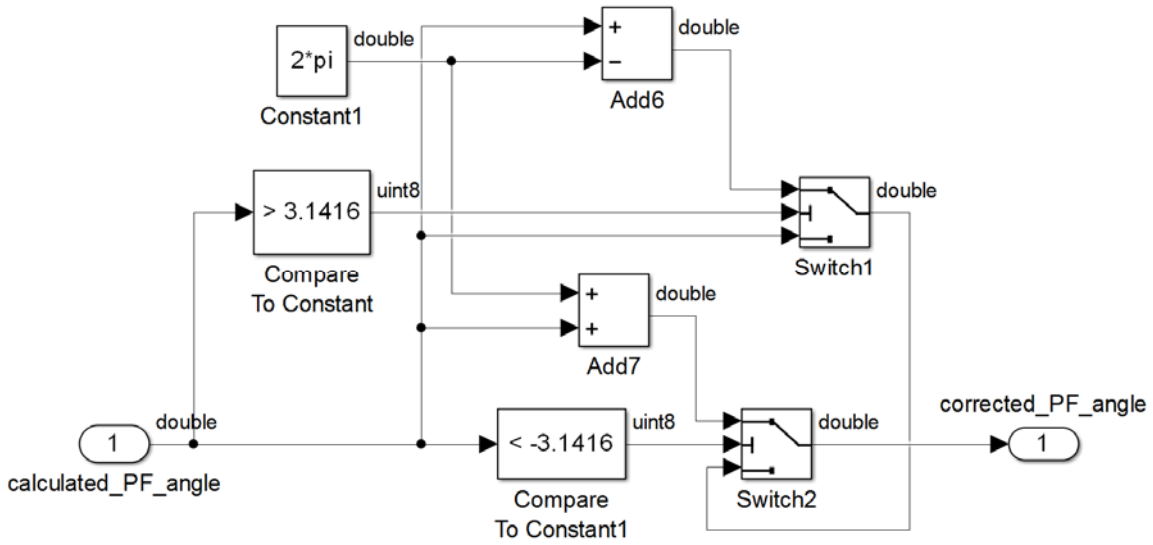

Figure 19. Simulink power factor angle error correction diagram.

The corrected power factor angle is then passed through a simple first-order low-pass filter transfer function as seen in Figure 14. The LPF softens the change in φ_{source} over time, which assists the *Closed-Loop Current Control* subsystem in smoothly adjusting the reference current amplitude I^*_{ems}. Plots of the corrected and filtered power factor angle are shown in Figure 20. Note from the plots that $\varphi_{source} < 0$ when the circuit is capacitive (0 s < time < 0.25 s) and $\varphi_{source} > 0$ when the circuit is inductive (time > 0.25 s). The load change is scheduled at precisely 0.25 s; however, the zero-crossing detection algorithm does not detect a change in $\theta_{i_{source}}$ until the end of the next zero-crossing event, which occurs one full period (1/60 s) later.

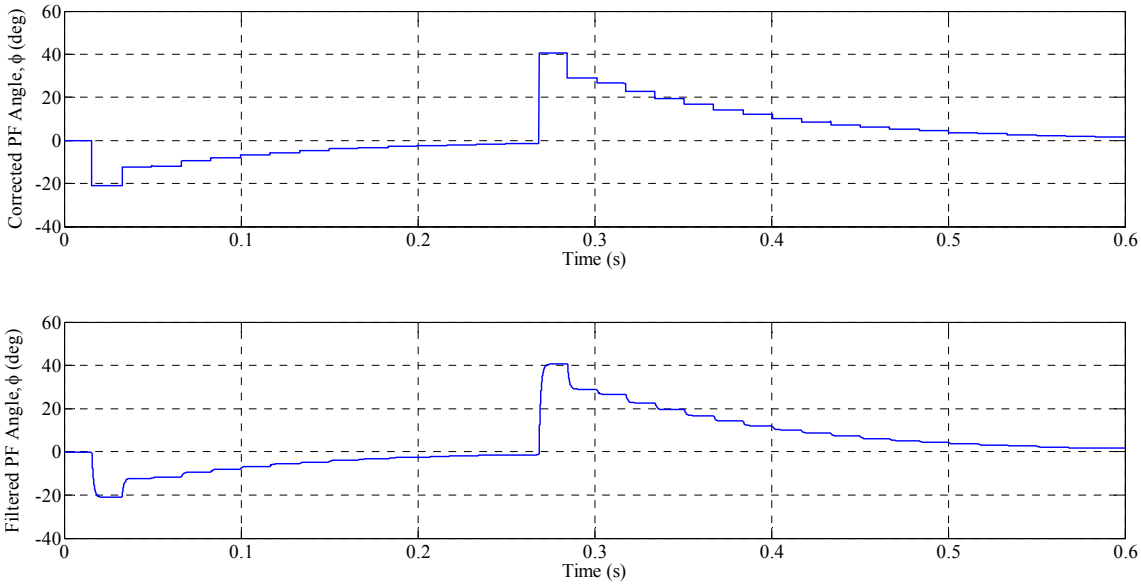

Figure 20. Corrected and filtered power factor angle plots.

3. Closed-Loop Current Control

The function of the Simulink *Closed-Loop Current Control* subsystem is to modify EMS output current i^*_{ems} by changing its amplitude I^*_{ems}. The closed-loop current control block diagram is shown in Figure 21. The diagram mathematically replicates the i^*_{ems} generation process described by the flow chart in Figure 13.

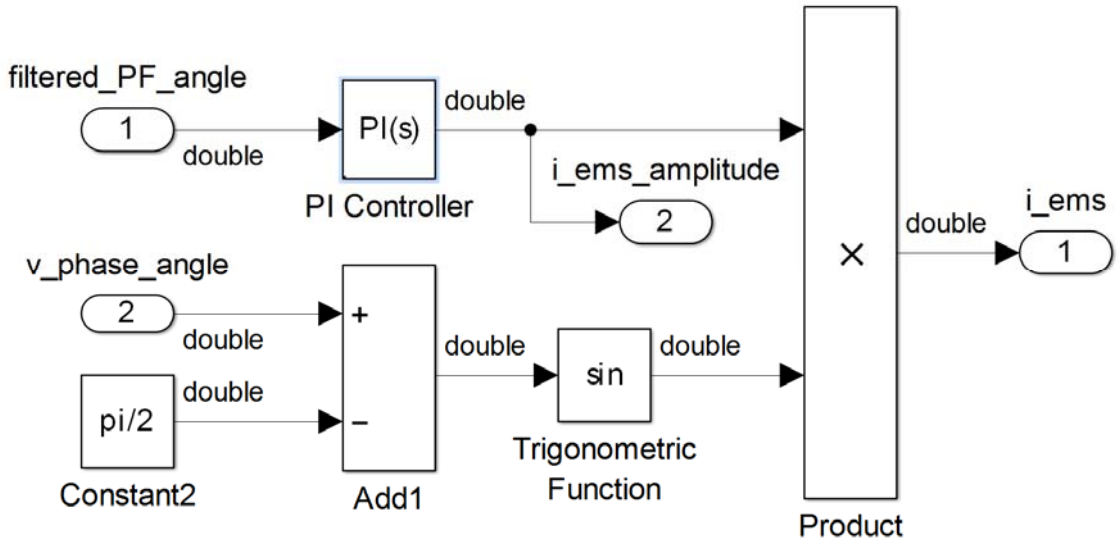

Figure 21. Simulink closed-loop current control diagram.

EMS current amplitude I^*_{ems} is produced as the output of the PI controller. The controller uses negative feedback to drive φ to zero. The fed-back output signal is reactive current i^*_{ems}, which is created by multiplying I^*_{ems} with a 1.0 A_{pk} continuous sinusoidal waveform generated in quadrature with v_{source}. The fed-back output signal thus has the form

$$i^*_{ems} = I^*_{ems} \sin\left(\theta_{v_{source}} - \pi/2\right) \tag{5}$$

where amplitude I^*_{ems} is adjusted by the PI controller to bring i_{source} in phase with v_{source}.

Changing the phase angle of i_{source} by adjusting the amplitude of i^*_{ems} is possible by Kirchhoff's Current Law (KCL). This is apparent when observing the flow of current through the PCC of the circuit in Figure 9. Given that $i^*_{ems} = i_{ems}$ for the simulation circuit, the KCL equation for i_{source} is

$$i_{source} = i_{load} + i_{cap} - i_{ems} \tag{6}$$

where positive i_{ems} describes the flow of EMS current into the PCC, hence the minus sign in Equation (6).

Plots of I^*_{ems} and φ_{source} versus time are displayed in Figure 22. The plots demonstrate the relationship between I^*_{ems} and φ_{source}—specifically how EMS current amplitude I^*_{ems} changes accordingly to pull i_{source} in phase with v_{source} (i.e., force φ_{source} to zero) thereby achieving a unity power factor at the grid. Also note that I^*_{ems} approaches unity as φ_{source} approaches zero. This occurs because no further change to i^*_{ems} is required when $\varphi_{source} = 0$. Observe that I^*_{ems} can be negative or positive depending on whether i_{source} leads or lags v_{source}, respectively.

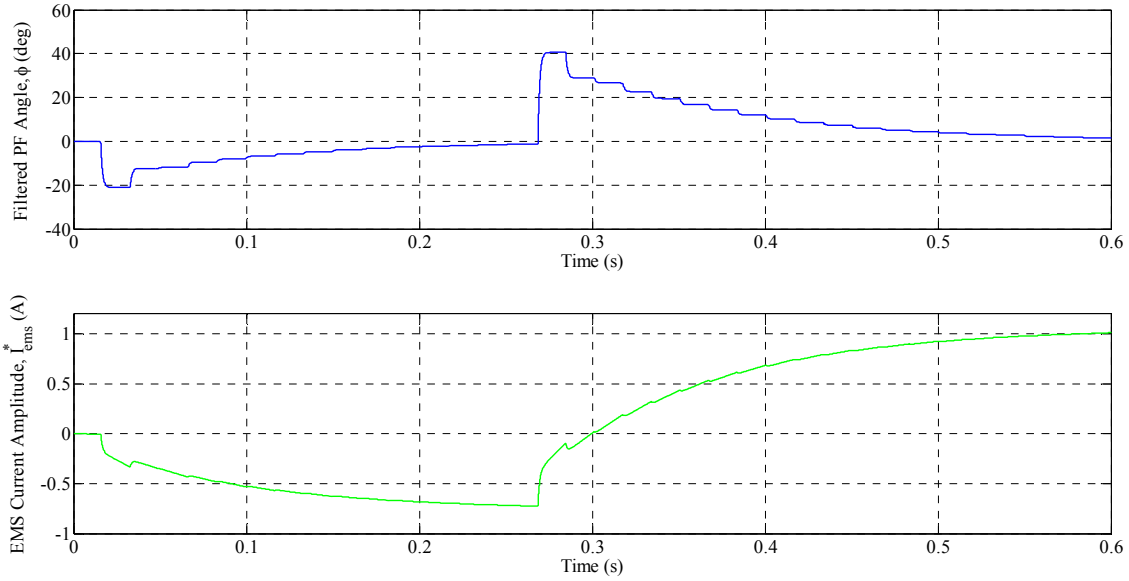

Figure 22. Changing EMS current amplitude to bring the source current in phase with the source voltage in order to achieve a unity power factor.

D. RESULTS

The simulation results are graphically displayed in Figure 23 and Figure 24. The figures demonstrate the system responses in terms of v_{source}, i_{source}, and i_{ems} for the resistive and inductive load cases exhibited in Figure 9. The results shown in Figure 23 are in response to the 85.7 Ω resistive load placed on the EMS at the start of the simulation. At 0.25 s, the 0.246 H inductive load is added to the circuit. The system response to the inductive load is illustrated in Figure 24. In both figures, v_{source} is scaled down by a factor of 50 in order to more adequately contrast the three signals. The voltage v_{source} still represents the 110 V_{rms} voltage supply provided by the grid.

At the start of the simulation, the circuit impedance is dominated by the 12 μF AC filter capacitor despite the active 85.7 Ω load. Hence, the overall circuit reactance is capacitive resulting in a leading grid power factor where initially $\varphi_{source} = -21^0$ as illustrated in Figure 23. The leading power factor implies that the filter capacitor is selling reactive power to the grid. The EMS compensates by generating an inductive i_{ems} that lags v_{source} by 90^0. This EMS effectively absorbs reactive power from the system in order to bring the i_{source} signal in phase with v_{source}. Notice that the amplitude of i_{ems}

gradually increases to 0.71 A_{pk} over 0.24 s until i_{ems} reaches steady-state conditions, which indicates that a unity power factor is achieved at the grid.

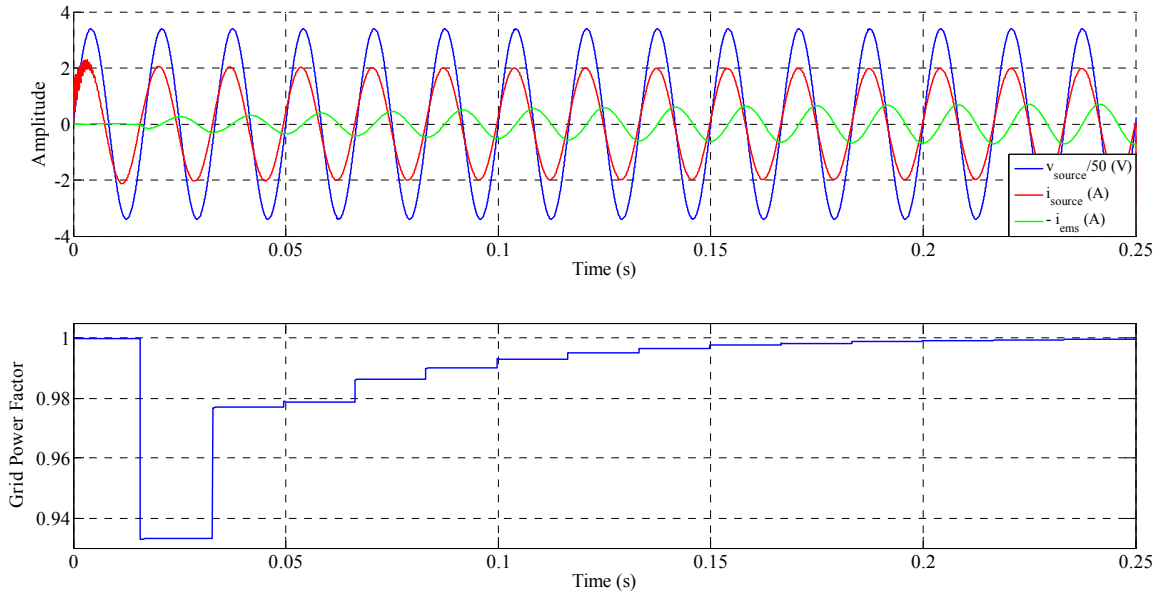

Figure 23. Grid power factor improvement for the purely resistive load case.

At 0.25 s, the 0.246 H inductive load is added to the system generating an overall inductive reactance in the circuit. The inductance demands reactive power from the grid causing a lagging grid power factor. The results in Figure 24 show i_{source} initially lagging v_{source} by 41^0 upon activation of the inductive load, which results in a grid power factor of just over 75%. The EMS compensates by acting as a capacitive load in delivering magnetizing VARs to the system. The EMS injects capacitive i_{ems} at the PCC where i_{ems} leads v_{source} by 90^0. By delivering reactive power to the system, the EMS gradually brings i_{source} into phase with v_{source}. In this case, the amplitude of i_{ems} increases to about 1.01 A_{pk} over 0.30 s until i_{ems} reaches steady-state conditions as a unity power factor is achieved at the grid. At this point, the EMS makes no further adjustment to i_{ems}.

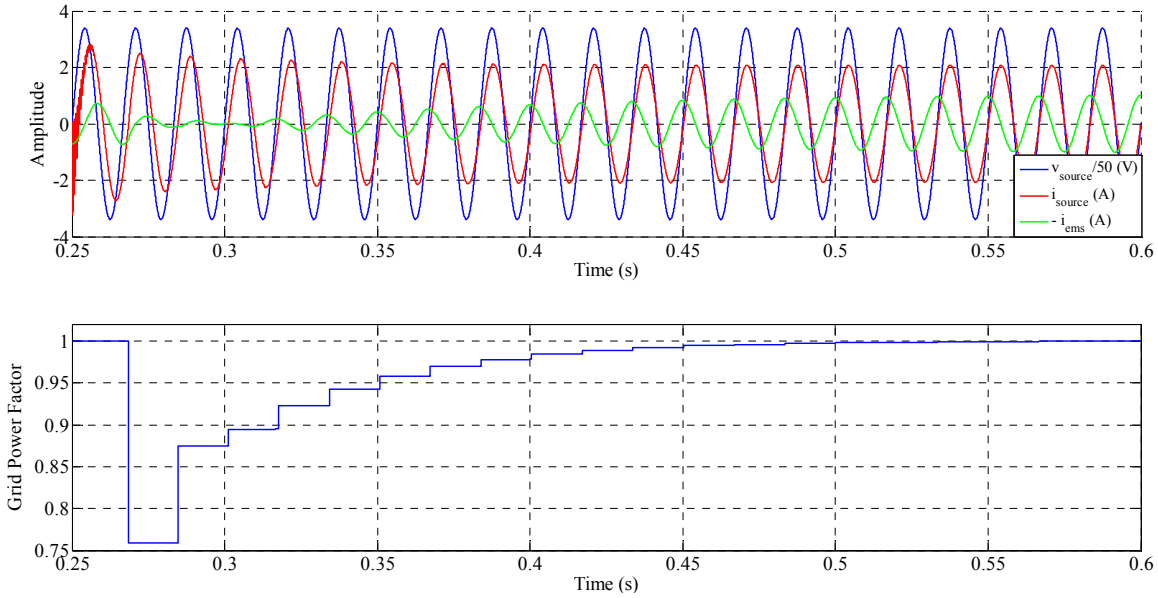

Figure 24. Grid power factor improvement for the inductive load case.

It is important to note that $-i_{ems}$ is used to represent EMS current in the simulation results shown in Figure 23 and Figure 24 in order to satisfy passive sign convention. Passive sign convention dictates that the reference direction for positive current flow is into a passive circuit component (i.e., a load). The load current i_{load} and filter capacitor current i_{cap} shown in Figures 8 and 9 are properly referenced using passive sign convention. This is also evidenced by Equation (6) using KCL; however, the simulation treats the EMS as an active circuit component (i.e., a source) whereby i_{ems} flows from the EMS to the PCC as shown in Figure 9. Hence, $-i_{ems}$ is given in Figures 23 and 24 since it portrays the positive flow of current into the EMS, which is consistent with the reference direction used in the simulation to describe positive current flow through all other loads.

THIS PAGE INTENTIONALLY LEFT BLANK

IV. LABORATORY EXPERIMENT

A. SETUP

The experiment was set up in the laboratory using the EMS hardware described in Chapter II. Recall that the experimental EMS design incorporates the power electronics circuitry shown in Figure 25, which involves the use of PWM to generate the IGBT gate signals of the H-bridge inverter. The main electric grid provided the 60 Hz, 110 V_{rms} AC source input to the EMS. Clamp-on probes were used to take source voltage and current measurements, which were captured using an oscilloscope. A 72 V_{DC} battery bank powered the 200 V_{DC} bus via the DC-DC boost converter shown in Figure 25. The DC bus provided the DC input voltage to the H-bridge inverter.

All discrete component values for the circuit in Figure 25 are given in Table 1. Also, a digital photograph of the EMS under test is shown in Figure 26.

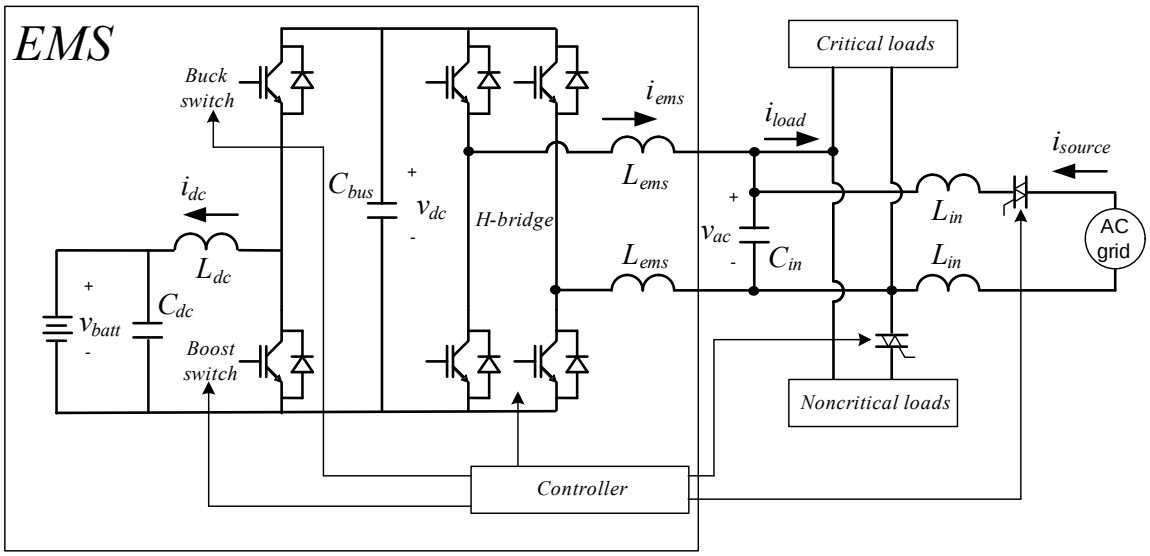

Figure 25. Experimental EMS power electronics circuit schematic.

Table 1. Discrete component values for the circuit in Figure 25.

Device	Value
AC grid	110 V_{rms}, 60 Hz
V_{batt}	72 V_{dc}
L_{in}	200 µH
L_{dc}	300 µH
L_{ems}	200 µH
C_{in}	12 µF
C_{dc}	500 µF
C_{bus}	2 mF
Load 1	85.7 Ω
Load 2	0.246 H

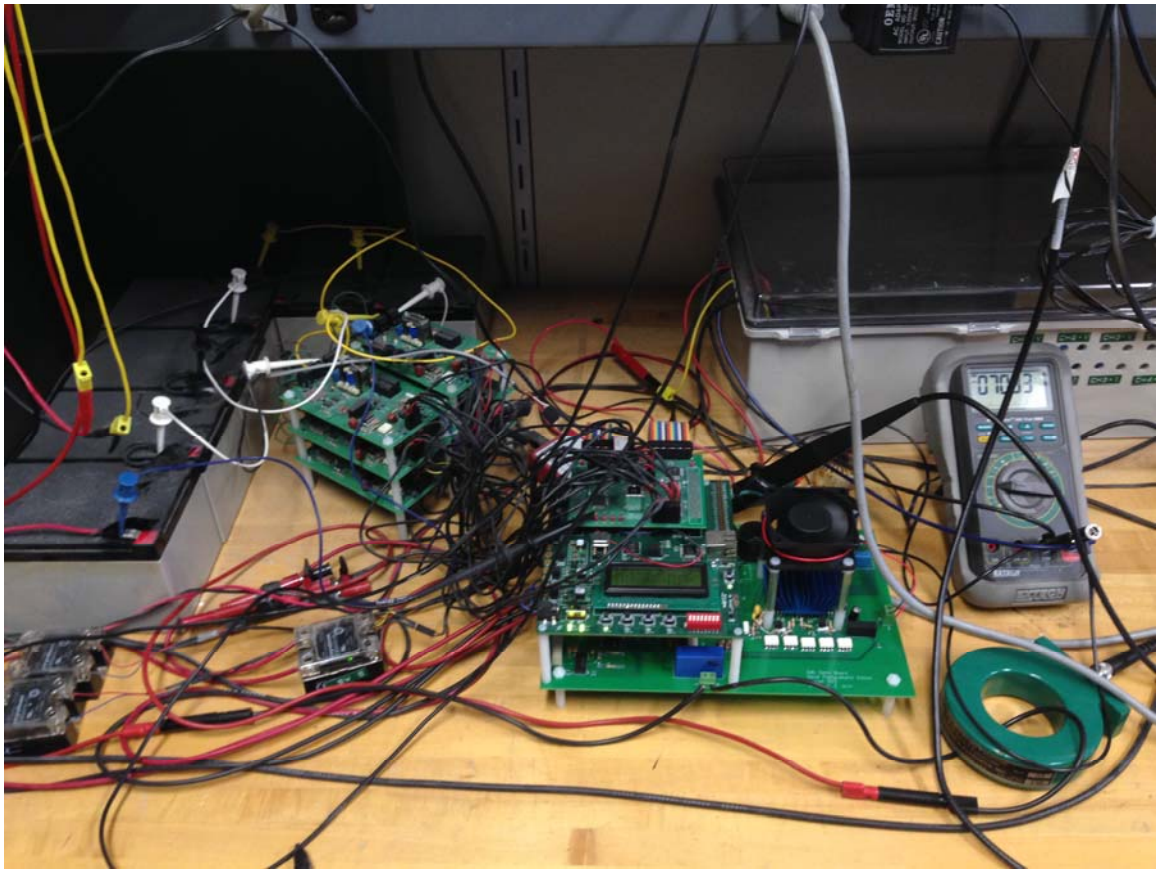

Figure 26. The EMS under test in the laboratory.

The oscilloscope, PC with Simulink and Xilinx software, and variable circuit loads are not shown in Figure 26; however, the variable load panels are shown in the photographs in Figure 27. The circuit loads were controlled by two load panels that connected to the EMS. Each panel consists of three parallel sets of three parallel resistors (300 Ω, 600 Ω, and 1200 Ω) or inductors (0.8 H, 1.6 H, and 3.2 H) to support up to three-phase load applications. The variable load boxes were accordingly configured to facilitate the experiment. This setup can be seen in Figure 27 where the appropriate resistor and inductor switches were activated to provide the 85.7 Ω and 0.246 H parallel loads used in the experiment.

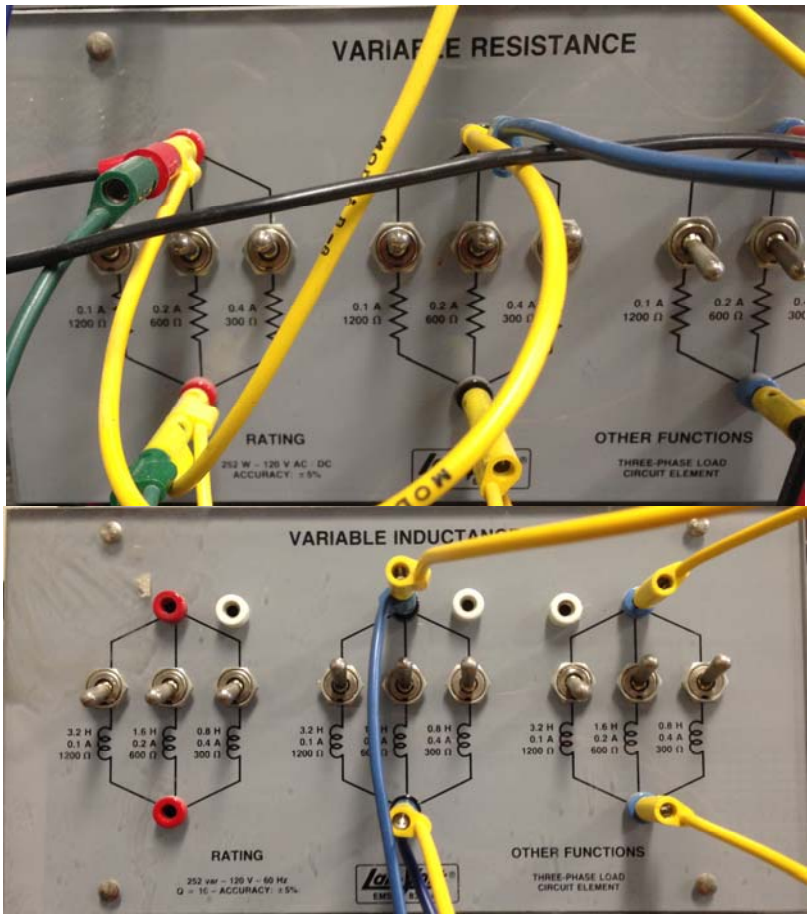

Figure 27. Variable load panels used in the experiment.

B. PROCEDURE

Implementation of the experiment was a straightforward process. Upon completing the lab setup, the Simulink simulation was compiled into VHDL code on a PC and uploaded to the FPGA development board on the EMS using Xilinx software. The VHDL code enabled the EMS to execute the power factor correction methodology developed in Simulink.

The purpose of the experiment was to validate simulation results for the compensation of an inductive power demand on the grid. Thus, both the 85.7 Ω resistive load and 0.246 H inductive load were effective at the start of the experiment in order to emulate circuit conditions similar to those modeled with Simulink upon activation of the inductive load at 0.25 s into the simulation.

EMS functionality permitted the manual activation and deactivation of i_{ems}; therefore, i_{ems} was not immediately turned on so that the effects of the inductive power demand on the grid could be observed and recorded using the oscilloscope. Once initial measurements were collected, i_{ems} was activated, and the resultant waveforms were captured. The resultant experimental data is presented in Figures 28–31.

Since the EMS did not possess a current sensor at the source as previously mentioned, the microcontroller was incapable of measuring $\theta_{i_{source}}$ and, therefore, could not conduct closed-loop control of reference current i^*_{ems}. The EMS could only generate a single i_{ems} signal from the H-bridge inverter. Consequently, the EMS was merely able to produce the 1.0 A_{pk} continuous quadrature current waveform shown in Figure 13 to compensate for a reactive power demand on the grid. Adjustments to I^*_{ems} based on changes to $\theta_{i_{source}}$ were not possible with the current hardware configuration. However, the purpose of the experiment was to demonstrate the potential of the EMS to compensate for a reactive power demand on the source using the method tested in simulation. This capability is confirmed by the experimental results.

C. RESULTS

The ohmic-inductive circuit load initally creates an overall inductive reactance in the circuit that results in a lagging power factor at the grid as expected. This is shown by the source voltage and current waveforms in Figure 28 where i_{source} lags v_{source} by approximately 30°, which translates into an 87% source power factor. This power factor is slightly improved over the 75% power factor initially realized in simulation; however, this discrepancy is expected since the simulation does not account for the many electronic devices that induce reactance throughout the EMS circuitry.

Notice also in Figure 28 that no reactive power compensation occurs since i_{ems} is not yet activated. There also appears to be small negative DC voltage component in the source voltage of about −0.34 V. This DC offset is a consequence of calibration error in the EMS voltage sensor since the equipment was not properly calibrated before the experiment was conducted. Also of note, the voltage and current waveforms shown in Figure 28 were created in MATLAB using data imported from the oscilloscope. The oscilloscope display of the very same waveforms is provided for reference in Figure 29.

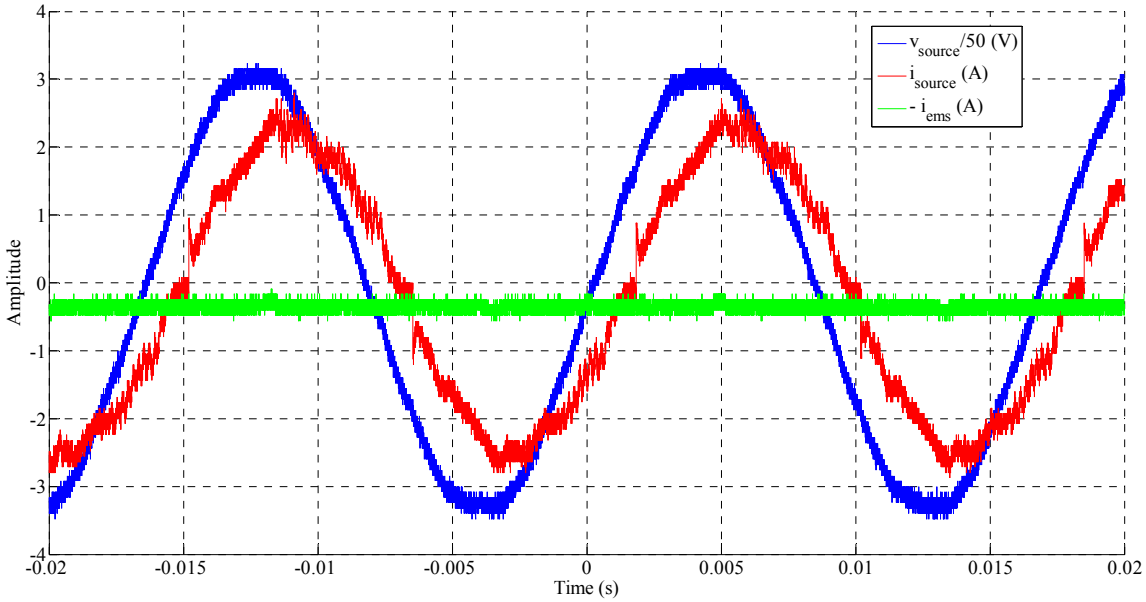

Figure 28. Source voltage and current when EMS current is off (MATLAB).

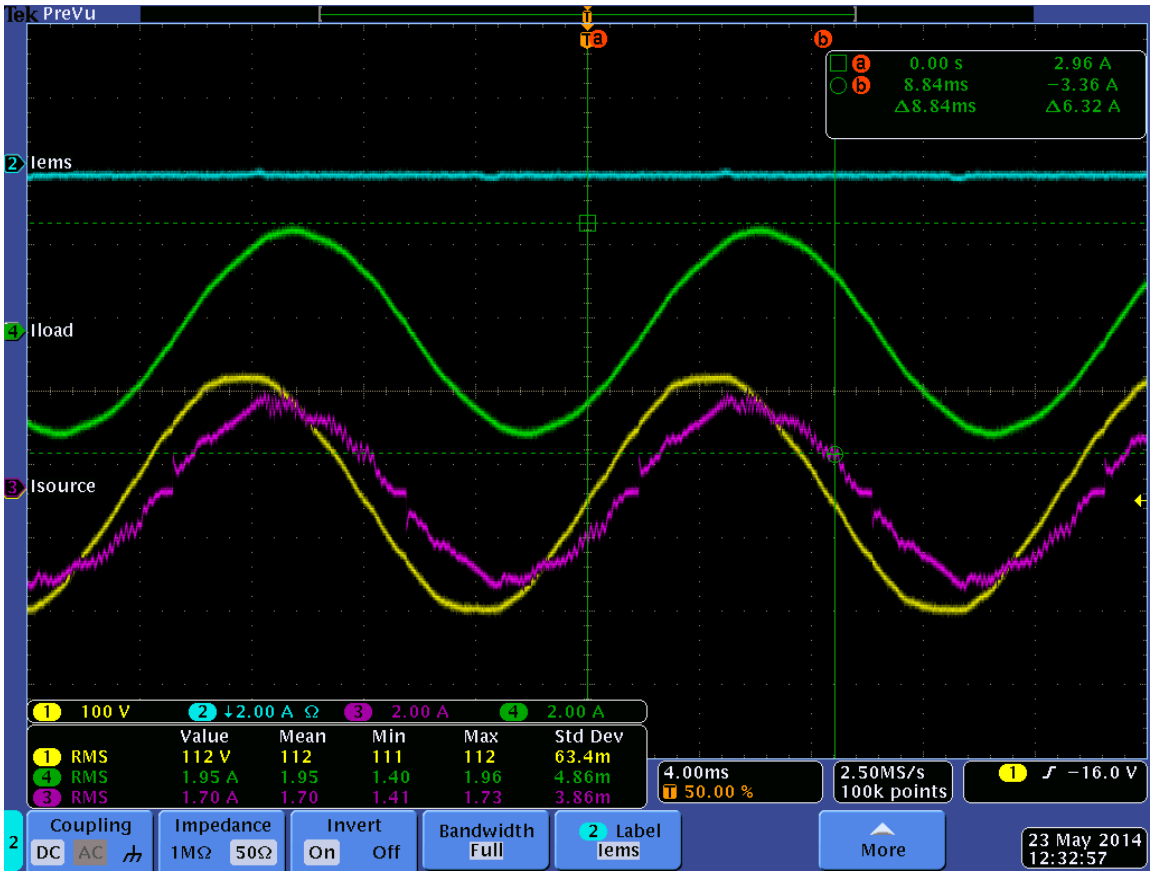

Figure 29. Source voltage and current when EMS current is off (oscilloscope).

Once i_{ems} is activated, capacitive power is delivered to the system causing the phase angle of i_{source} to shift until i_{source} slightly leads v_{source}. This over-compensation of reactive power to the grid occurs because the EMS is currently incapable of employing a proper closed-loop current control scheme. The EMS merely produces a constant 1.0 A_{pk} sinusoidal i_{ems} signal in quadrature with the source voltage. The amplitude of i_{ems} does not change without a PI controller, and a leading power factor occurs at the grid. This situation is illustrated in Figure 30. A proper closed-loop current control method would otherwise adjust the amplitude of i_{ems} so as to pull i_{source} in phase with v_{source}.

Notice in Figures 30 and 31 that $-i_{ems}$ is again used to represent EMS current. This is because the EMS executes the same power factor correction algorithm used by the simulation whereby the EMS is treated as a current source in accordance with passive

sign convention; thus, presenting $-i_{ems}$ in the experiment results serves to characterize the EMS as a circuit load, which ensures consistency in referencing the direction of positive flow of current from the PCC to the loads.

The presence of harmonics in the i_{ems} signal is also obvious from the i_{ems} waveforms shown in Figures 30 and 31. The harmonics stem from the PWM switching scheme used by the EMS to generate i_{ems}. These harmonic signatures are not evident in the simulation results since the circuit modeled in Simulink disregards PWM associated with the EMS's power electronics.

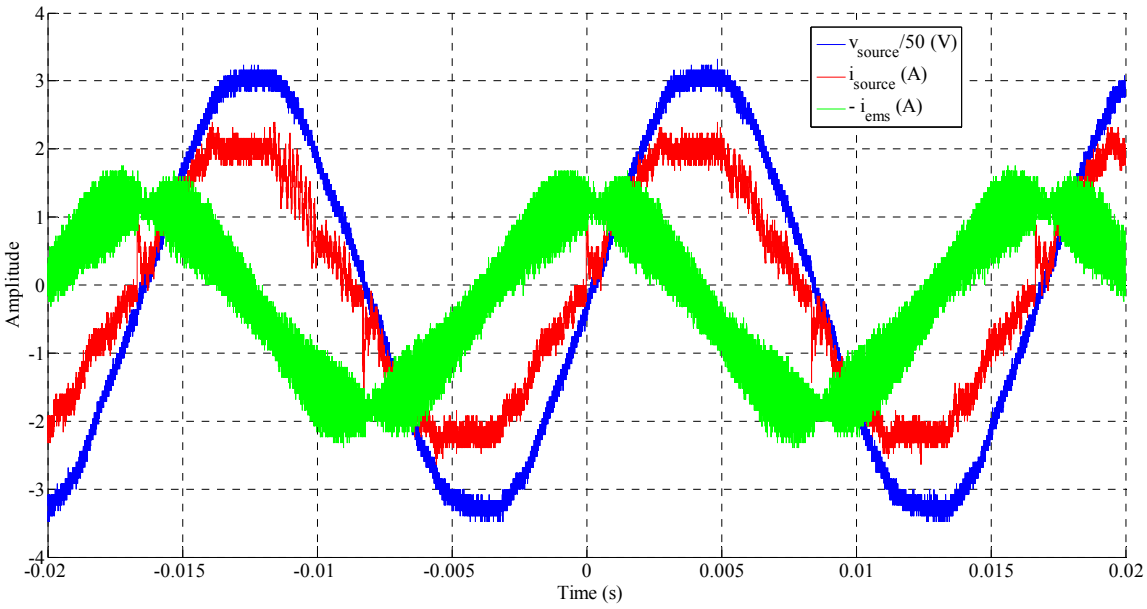

Figure 30. Source voltage and current when EMS current is on (MATLAB).

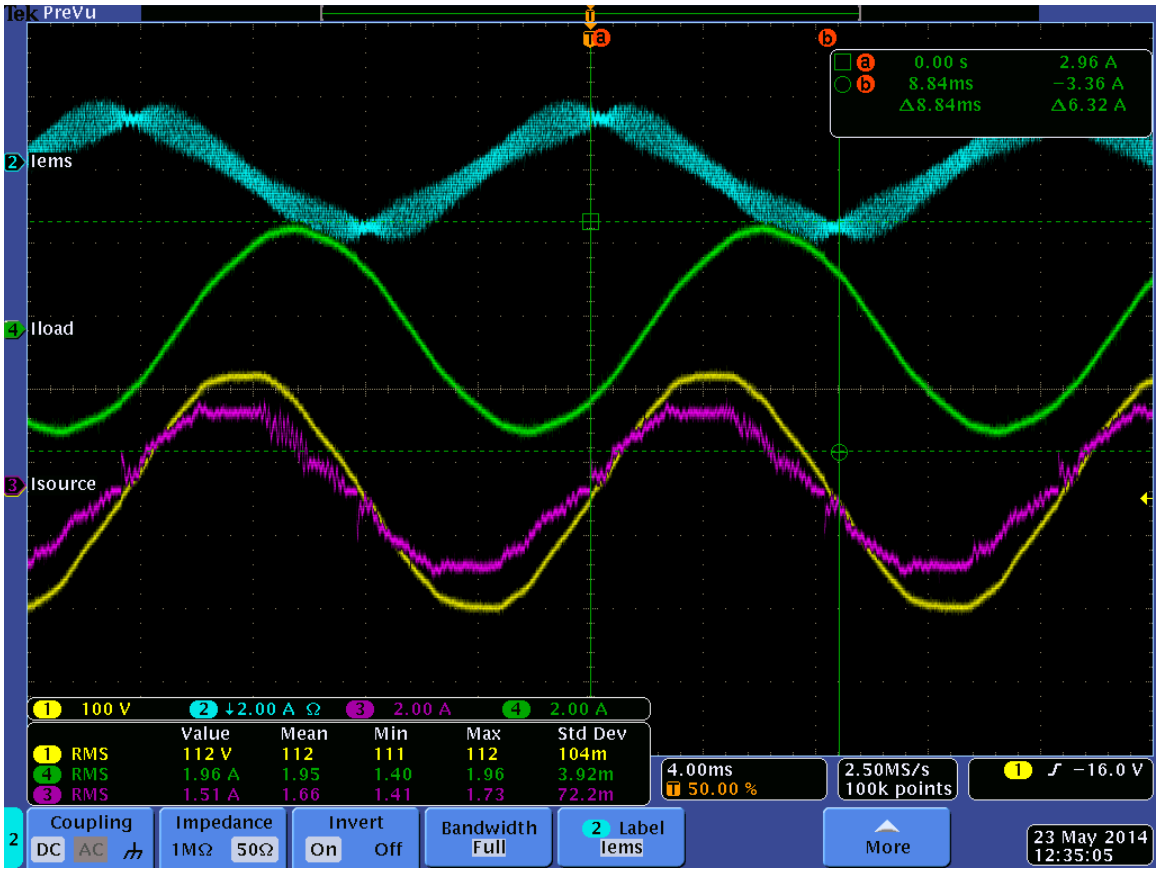

Figure 31. Source voltage and current when EMS current is on (oscilloscope).

V. CONCLUSIONS AND RECOMMENDATIONS

A. CONCLUSIONS

Reactive power compensation and power factor improvement are not new engineering concepts. Controlling the generation, transmission, and distribution of reactive energy in delivering quality power to the consumer is essential to increasing energy efficiency and reducing energy costs. As a result, various methods for achieving a unity power factor at the source have been developed and improved over time.

A particular means of compensating for a reactive power demand on the grid was examined in this thesis whereby an additional capability to a particular EMS was proposed that enabled the EMS to operate as current source in compensating for a reactive power demand on the grid. This was accomplished by first using a Simulink-based zero-crossing detection algorithm to determine the power factor angle between the source voltage and current. The appropriate amount of reactive current was subsequently injected into the system and adjusted using a closed-loop current control scheme that brought the source current in phase with the source voltage thereby eliminating any reactive power demand on the grid. A Simulink model of the process was initially developed in order to forecast the system's response to both capacitive and inductive power demands on the grid. The process was then confirmed in a laboratory using the actual EMS.

It is important to remember that the Simulink model was simplified so as to isolate the reactive power compensation process for analysis by specifically neglecting to model the EMS's power electronics systems. The PWM scheme and related PI control of the H-bridge IGBT gate signals in particular were disregarded. The EMS was thus modeled as a constant current source. This eased the complexity of the simulation design but created disparities between model functionality and actual EMS operation, which caused some dissimilarity between simulation and experimental results.

For example, no harmonics were observed in the simulation representation of i_{ems} since the effects of the EMS's power electronics were disregarded by the circuit modeled

in Simulink. Likewise, additional circuit reactance associated with discrete electronic components was not observed in the simulation and, therefore, did not affect the reactive power demand on the grid. Nevertheless, the results verified the ability of the EMS to apply the Simulink-based power factor correction algorithm in compensating for a reactive power demand on the grid.

Moreover, the EMS hardware did not possess a current sensor at the source, so no closed-loop control of i_{ems} was implemented in the laboratory. The EMS was consequently unable to adjust the amplitude of i_{ems} in correcting the source power factor angle. The EMS still demonstrated the ability to improve the power factor at the source, but a unity power factor could not be achieved without the use of closed-loop current control. An EMS hardware upgrade is currently planned that will improve the functionality of the EMS.

B. RECOMMENDATIONS

The results presented in this thesis built confidence in the ability of the EMS to compensate for a reactive power demand on the grid; however, improving the simulation and experiment could potentially facilitate a better understanding of the EMS's capabilities. It would be advantageous, for example, to repeat the experiment once a source current sensor is installed in the EMS in order to fully validate the reactive power compensation process designed in Simulink. Also, the simulation could be further developed to simulate the EMS's power electronics architecture, which includes the PWM and controller required to operate the H-bridge inverter. Combining the two aforementioned efforts into a single project might enable a better comparison of the simulation and experiment results.

Additionally, future research into other reactive power compensation methods involving the EMS would add depth to its functionality and facilitate a comparative analysis of the different methods. Investigating the system's response to various reactive power demand scenarios might also assist in identifying the advantages and limitations of each method. These results could then be used to develop a decision-making algorithm

that enables the EMS to choose an optimal power factor improvement process when faced with varying power supply and demand situations.

One example of a potential alternative to the reactive power compensation method presented in this thesis is the use of a phase-locked loop (PLL) control scheme to detect and match the source current and voltage phase angles. While developing a PLL control scheme may be a more complex design effort, it could potentially alleviate the numerical integration error associated with zero-crossing detection when signal transients are present in the source current.

THIS PAGE INTENTIONALLY LEFT BLANK

APPENDIX. MATLAB M-FILES

A. SIMULATION INITIAL CONDITIONS FILE

```
% Michael Prato
% Reactive Power Compensation Using an EMS
% Initial Conditions File

clear all;
clc;
close all;
V_source=120*sqrt(2);   % Source voltage (V peak)
freq=2*pi*60;           % Source voltage frequency (rad)
Kp=2/4;                 % Proportional gain of the PI controller
Ki=100/4;               % Integral gain of the PI controller
R_load=85.714;          % Resistive load (ohms)
L_load=0.246;           % Inductive load (H)
R_of_L_load=5;          % Resistance of the inductor (ohms)
Rin=0.01;               % Internal resistance (ohms)
L_fil=400e-6;           % Filter inductor (H)
C_fil=12e-6;            % Filter capacitor (F)
tstep = 0.5e-5;         % Step size (sec)
tstop = 0.6;            % Sim length (sec)
```

B. SIMULATION OUTPUT PLOT FILE

```
% Michael Prato
% Reactive Power Compensation Using an EMS
% Output Plot File
% Replicates oscilloscope waveforms based on output data files
collected from the oscilloscope

v_cap=data_out(:,1);
i_source=data_out(:,2);
i_ems=data_out(:,3);
i_load=data_out(:,4);
filtered_PF_angle=data_out(:,5);
v_source=data_out(:,6);
i_ems_amplitude=data_out(:,7);
i_phase_angle=data_out(:,8);
v_phase_angle=data_out(:,9);
calculated_PF_angle=data_out(:,10);
corrected_PF_angle=data_out(:,11);

figure('name','Reactive Power Compensation');
hold on;
plot(time,v_source/50,'b','linewidth',1.5);
plot(time,i_source,'r','linewidth',1.5)
plot(time,-i_ems,'g','linewidth',1.5)
xlabel('Time (s)','FontSize',20); ylabel('Amplitude','FontSize',20);
xlim([0 tstop]);
legend('v_s_o_u_r_c_e/50 (V)','i_s_o_u_r_c_e (A)','- i_e_m_s (A)');
```

```
grid on;
hold off;

figure('name','Grid Power Factor');
plot(time,cos(calculated_PF_angle),'linewidth',2);
xlabel('Time (s)','FontSize',20); ylabel('Grid Power
Factor','FontSize',20);
xlim([0 tstop]); ylim([0.75 1.02]);
grid on;

figure('name','Reactive Power Compensation by Achieving a Unity PF,
Ohmic Load');
subplot(2,1,1); grid on;
hold on;
plot(time,v_source/50,'b','linewidth',2);
plot(time,i_source,'r','linewidth',2)
plot(time,-i_ems,'g','linewidth',2)
%title('Purely Resistive Load (85.7 \Omega)','FontSize',20);
xlim([0 0.25]);
xlabel('Time (s)','FontSize',20); ylabel('Amplitude','FontSize',20);
legend('v_s_o_u_r_c_e/50 (V)','i_s_o_u_r_c_e (A)','- i_e_m_s
(A)','location','south');
subplot(2,1,2);
plot(time,cos(calculated_PF_angle),'linewidth',2); grid on;
xlabel('Time (s)','FontSize',20); ylabel('Grid Power
Factor','FontSize',20);
%title('Power Factor','FontSize',20);
xlim([0 0.25]); ylim([0.93 1.005]);

figure('name','Reactive Power Compensation by Achieving a Unity PF,
Inductive Load');
subplot(2,1,1); grid on;
hold on;
plot(time,v_source/50,'b','linewidth',2);
plot(time,i_source,'r','linewidth',2)
plot(time,-i_ems,'g','linewidth',2)
%title('Inductive Load (0.246 H) Added to the Circuit at t = 0.25
s','FontSize',20);
xlabel('Time (s)','FontSize',20); ylabel('Amplitude','FontSize',20);
xlim([0.25 tstop]);
legend('v_s_o_u_r_c_e/50 (V)','i_s_o_u_r_c_e (A)','- i_e_m_s
(A)','location','south');
subplot(2,1,2);
plot(time,cos(calculated_PF_angle),'linewidth',2); grid on;
xlabel('Time (s)','FontSize',20); ylabel('Grid Power
Factor','FontSize',20);
%title('Power Factor','FontSize',20);
xlim([0.25 tstop]); ylim([0.75 1.02]);

figure('name','Phase Angles')
plot(time,v_phase_angle*180/pi,'b','linewidth',1.5);
hold on;
plot(time,i_phase_angle*180/pi,'g','linewidth',1.5);
hold off;
```

```
xlabel('Time (s)','FontSize',16); ylabel('Phase Angle, \theta
(deg)','FontSize',16);
legend('\theta_v_{_s_o_u_r_c_e}','\theta_i_{_s_o_u_r_c_e}','FontSize',1
6);
xlim([0 tstop]); ylim([0 410]);
grid on;

figure('name','Phase Angles from t=[0,0.6]sec')
subplot(2,1,1); grid;
hold on;
plot(time,v_phase_angle*180/pi,'b','linewidth',1.5);
plot(time,i_phase_angle*180/pi,'g','linewidth',1.5);
hold off;
title('Resistive Load (85.7 \Omega)','FontSize',20);
xlim([0 0.25]);
xlabel('Time (s)','FontSize',16); ylabel('Phase Angle, \theta
(deg)','FontSize',20);
legend('\theta_v_{_s_o_u_r_c_e}','\theta_i_{_s_o_u_r_c_e}');
subplot(2,1,2); grid;
hold on;
plot(time,v_phase_angle*180/pi,'b','linewidth',1.5);
plot(time,i_phase_angle*180/pi,'g','linewidth',1.5);
hold off;
title('Inductive Load (0.246 H) Added to the Circuit at t = 0.25
s','FontSize',20);
xlim([0.25 tstop]);
xlabel('Time (s)','FontSize',16); ylabel('Phase Angle, \theta
(deg)','FontSize',20);
legend('\theta_v_{_s_o_u_r_c_e}','\theta_i_{_s_o_u_r_c_e}');

figure('name','Phase Angles from t=[0,0.35]sec')
subplot(2,1,1); grid;
hold on;
plot(time,v_phase_angle*180/pi,'b','linewidth',2);
plot(time,i_phase_angle*180/pi,'g','linewidth',2);
hold off;
title('Resistive Load (85.7 \Omega)','FontSize',20);
xlim([0 0.1]);
xlabel('Time (s)','FontSize',20); ylabel('Phase Angle, \theta
(deg)','FontSize',20);
legend('\theta_v_{_s_o_u_r_c_e}','\theta_i_{_s_o_u_r_c_e}','location','
southeast');
subplot(2,1,2); grid;
hold on;
plot(time,v_phase_angle*180/pi,'b','linewidth',2);
plot(time,i_phase_angle*180/pi,'g','linewidth',2);
hold off;
title('Inductive Load (0.246 H) Added to the Circuit at t = 0.25
sec','FontSize',20);
xlim([0.25 0.35]);
xlabel('Time (s)','FontSize',16); ylabel('Phase Angle, \theta
(deg)','FontSize',20);
legend('\theta_v_{_s_o_u_r_c_e}','\theta_i_{_s_o_u_r_c_e}');
```

```
figure('name','Calculated PF Angle Between Source Voltage and Source
Current')
plot(time,calculated_PF_angle*180/pi,'b','linewidth',2);
xlabel('Time (s)','FontSize',20); ylabel('Calculated PF Angle, \phi
(deg)','FontSize',20);
grid on; xlim([0 tstop]);

figure('name','Corrected and Filtered Power Factor Angle')
subplot(2,1,1),plot(time,corrected_PF_angle*180/pi,'b','linewidth',2);
grid; xlim([0 tstop]);
xlabel('Time (s)','FontSize',20); ylabel('Corrected PF Angle, \phi
(deg)','FontSize',20);
%legend('Unfiltered \phi (\theta_v_{_s_o_u_r_c_e} -
\theta_i_{_s_o_u_r_c_e})','location','south');
subplot(2,1,2),plot(time,filtered_PF_angle*180/pi,'b','linewidth',2);
grid; xlim([0 tstop]);
xlabel('Time (s)','FontSize',20); ylabel('Filtered PF Angle, \phi
(deg)','FontSize',20);
%legend('Filtered \phi (\theta_v_{_s_o_u_r_c_e} -
\theta_i_{_s_o_u_r_c_e})','location','south');
grid on;

figure('name','Power Factor Angle and EMS Current Amplitude')
subplot(2,1,1),plot(time,filtered_PF_angle*180/pi,'b','linewidth',2);
grid; xlim([0 tstop]);
xlabel('Time (s)','FontSize',20); ylabel('Filtered PF Angle, \phi
(deg)','FontSize',20);
%legend('Filtered \phi (\theta_v_{_s_o_u_r_c_e} -
\theta_i_{_s_o_u_r_c_e})','location','south');
subplot(2,1,2),plot(time,i_ems_amplitude,'g','linewidth',2); grid;
xlim([0 tstop]);
xlabel('Time (s)','FontSize',20); ylabel('EMS Current Amplitude,
I^*_e_m_s (A)','FontSize',20);
grid on;
```

C. EXPERIMENT OUTPUT PLOT FILE

```
% Michael Prato
% Reactive Power Compensation Using an EMS
% Oscilloscope Output Plot File

Clc;
clear all;
close all;

data_vac=xlsread('Tek_CH1_Wfm.csv');
data_iems=xlsread('Tek_CH2_Wfm.csv');
data_isource=xlsread('Tek_CH3_Wfm.csv');
data_iload =xlsread('Tek_CH4_Wfm.csv');
len = length(data_vac);

time_vec=data_vac(15:len,1);
vac=data_vac(15:len,2);
iems=data_iems(15:len,2);
```

```
iload=data_iload(15:len,2);
isource=data_isource(15:len,2);
tmin=time_vec(1);
tmax=max(time_vec);

data_vac2=xlsread('Tek_CH1_Wfmb.csv');
data_iems2=xlsread('Tek_CH2_Wfmb.csv');
data_isource2=xlsread('Tek_CH3_Wfmb.csv');
data_iload2 =xlsread('Tek_CH4_Wfmb.csv');
len = length(data_vac2);

time_vec2=data_vac2(15:len,1);
vac2=data_vac2(15:len,2);
iems2=data_iems2(15:len,2);
iload2=data_iload2(15:len,2);
isource2=data_isource2(15:len,2);
tmin2=time_vec(1);
tmax2=max(time_vec);

figure(1);
subplot(2,1,1), plot(time_vec,vac/50);
hold on;
plot(time_vec,isource,'r');
hold off;
xlabel('Time (s)');
ylabel('Amplitude');
legend('v_s_o_u_r_c_e/50 (V)','i_s_o_u_r_c_e
(A)','Location','Northeast'); grid on;
axis([tmin tmax -4 4]);

subplot(2,1,2),plot(time_vec,iems,'g',time_vec,iload,'m');
xlabel('Time (s)');
ylabel('Amplitude');
grid on;
legend('-i_e_m_s (A)','i_l_o_a_d (A)','Location','Northeast');
axis([tmin tmax -4 4]);

temp1=get(gcf,'position');
temp2=temp1+[-500, 0, temp1(3)*1.5, 0 ];
set(gcf,'position',temp2);
saveas(gcf,'figure1','tif');
print(gcf,'-dtiff','-r350','figure1');

figure(2);
subplot(2,1,1), plot(time_vec2,vac2/50);
hold on;
plot(time_vec2,isource2,'r');
hold off;
xlabel('Time (s)');
ylabel('Amplitude');
legend('v_s_o_u_r_c_e/50 (V)','i_s_o_u_r_c_e
(A)','Location','Northeast');
grid on;
axis([tmin tmax -4 4]);
```

```
subplot(2,1,2),plot(time_vec2,iems2,'g',time_vec2,iload2,'m');
xlabel('Time (s)');
ylabel('Amplitude');
grid on;
legend('-i_e_m_s (A)','i_l_o_a_d (A)','Location','Northeast');
axis([tmin tmax -4 4]);

temp1=get(gcf,'position');
temp2=temp1+[-500, 0, temp1(3)*1.5, 0 ];
set(gcf,'position',temp2);
saveas(gcf,'figure2','tif');
print(gcf,'-dtiff','-r350','figure2');

figure(3);
hold on;
plot(time_vec2,vac/50);
plot(time_vec2,isource,'r');
plot(time_vec2,iems,'g');
hold off;
xlabel('Time (s)');
ylabel('Amplitude');
legend('v_s_o_u_r_c_e/50 (V)','i_s_o_u_r_c_e (A)','- i_e_m_s
(A)','Location','Northeast');
grid on;
axis([tmin tmax -4 4]);

temp1=get(gcf,'position');
temp2=temp1+[-500, 0, temp1(3)*1.5, 0 ];
set(gcf,'position',temp2);
saveas(gcf,'figure3','tif');
print(gcf,'-dtiff','-r350','figure3');

figure(4);
hold on;
plot(time_vec2,vac2/50);
plot(time_vec2,isource2,'r');
plot(time_vec2,iems2,'g');
hold off;
xlabel('Time (s)');
ylabel('Amplitude');
legend('v_s_o_u_r_c_e/50 (V)','i_s_o_u_r_c_e (A)','- i_e_m_s
(A)','Location','Northeast');
grid on;
axis([tmin tmax -4 4]);

temp1=get(gcf,'position');
temp2=temp1+[-500, 0, temp1(3)*1.5, 0 ];
set(gcf,'position',temp2);
saveas(gcf,'figure4','tif');
print(gcf,'-dtiff','-r350','figure4');

figure(5);
hold on;
```

```
plot(time_vec,vac/50);
plot(time_vec,isource,'r');
plot(time_vec,iems,'g');
plot(time_vec,iload,'m');
hold off;
xlabel('Time (s)');
ylabel('Amplitude');
legend('v_s_o_u_r_c_e/50 (V)','i_s_o_u_r_c_e (A)','-i_e_m_s
(A)','i_l_o_a_d (A)','Location','Northeast');
grid on;
axis([tmin tmax -4 4]);

temp1=get(gcf,'position');
temp2=temp1+[-500, 0, temp1(3)*1.5, 0 ];
set(gcf,'position',temp2);
saveas(gcf,'figure5','tif');
print(gcf,'-dtiff','-r350','figure3');

figure(6);
hold on;
plot(time_vec,vac2/50);
plot(time_vec,isource2,'r');
plot(time_vec,iems2,'g');
plot(time_vec,iload2,'m');
hold off;
xlabel('Time (s)');
ylabel('Amplitude');
legend('v_s_o_u_r_c_e/50 (V)','i_s_o_u_r_c_e (A)','-i_e_m_s
(A)','i_l_o_a_d (A)','Location','Northeast');
grid on;
axis([tmin tmax -4 4]);

temp1=get(gcf,'position');
temp2=temp1+[-500, 0, temp1(3)*1.5, 0 ];
set(gcf,'position',temp2);
saveas(gcf,'figure6','tif');
print(gcf,'-dtiff','-r350','figure4');
```

THIS PAGE INTENTIONALLY LEFT BLANK

LIST OF REFERENCES

[1] *United States Marine Corps Expeditionary Energy Strategy and Implementation Plan*, Washington, DC: Marine Corps Expeditionary Energy Office, 2011.

[2] W. Hofmann, and J. Schlabbach, W. Just, *Reactive Power Compensation: A Practical Guide*. Chichester, UK: John Wiley & Sons, Ltd., 2012.

[3] S. Booth, J. Barnett, K. Burman, J. Hambrick, and R. Westby, "Net zero energy military installations: A guide to assessment and planning," National Renewable Energy Lab., Golden, CO, Tech. Rep. NREL/TP-7A2–48876, Aug. 2010.

[4] Commission Staff Report, "Payment for reactive power," Federal Energy Regulatory Commission, Washington, DC, Rep. AD14–7, Apr. 22, 2014.

[5] Simulink® by MathWorks [Online]. http://www.mathworks.com/products/simulink

[6] R. L. Kelly, "Optimizing gas generator efficiency in a forward operating base using an energy management system," M.S. thesis, Dept. Elect. Comp. Eng., Naval Postgraduate School, Monterey, CA, 2013.

[7] A. J. Metzcus, "H-bridge inverter loading analysis for an energy management system," M.S. thesis, Dept. Elect. Comp. Eng., Naval Postgraduate School, Monterey, CA, 2013.

[8] N. J. Peck, "Peak power control with an energy management system," M.S. thesis, Dept. Elect. Comp. Eng., Naval Postgraduate School, Monterey, CA, 2013.

[9] R. Carnieletto, D. I. Brandão, S. Suryanarayanan, F. A. Farret, and M. G. Simões, "Smart grid initiative," *IEEE Ind. Appl. Mag.*, vol. 17, no. 5, pp. 27–35, Sep./Oct. 2011.

[10] J. He, Y. W. Li, F. B. Blaabjerg, and X. Wang, "Active harmonic filtering using current-controlled, grid-connected DG units with closed-loop power control," *IEEE Trans. Power Electron.*, vol. 29, no. 2, pp. 642–653, Feb. 2014.

[11] G. Oriti, A. L. Julian, and N. J. Peck, "Power electronics enabled energy management systems," in *Proceedings of IEEE Applied Power Electronics Conference*, Long Beach, CA, Mar. 2013, pp. 3224–3231.

[12] *Xilinx® system generator for DSP: Getting started guide (v14.3)* [Online]. Available: http://www.xilinx.com/support/

[13] N. Mohan, T. M. Undeland, and W. P. Robbins, *Power Electronics: Converters, Applications, and Design,* 3rd ed. New York: John Wiley & Sons, Inc., 2003.

THIS PAGE INTENTIONALLY LEFT BLANK

INITIAL DISTRIBUTION LIST

1. Defense Technical Information Center
   Ft. Belvoir, Virginia

2. Dudley Knox Library
   Naval Postgraduate School
   Monterey, California